

Turbulence Dissipation and Particle Injection in Non-Linear Diffusive Shock Acceleration with Magnetic Field Amplification

Andrey Vladimirov

*Physics Department, North Carolina State University, Box 8202, Raleigh, NC 27695;
avladim@ncsu.edu*

Andrei M. Bykov

*Department of Theoretical Astrophysics, Ioffe Physical-Technical Institute, St. Petersburg,
Russia; byk@astro.ioffe.ru*

and

Donald C. Ellison

*Physics Department, North Carolina State University, Box 8202, Raleigh, NC 27695;
don_ellison@ncsu.edu*

ABSTRACT

The highly amplified magnetic fields suggested by observations of some supernova remnant (SNR) shells are most likely an intrinsic part of efficient particle acceleration by shocks. This strong turbulence, which may result from cosmic ray driven instabilities, both resonant and non-resonant, in the shock precursor, is certain to play a critical role in self-consistent, nonlinear models of strong, cosmic ray modified shocks. Here we present a Monte Carlo model of nonlinear diffusive shock acceleration (DSA) accounting for magnetic field amplification through resonant instabilities induced by accelerated particles, and including the effects of dissipation of turbulence upstream of a shock and the subsequent precursor plasma heating. Feedback effects between the plasma heating due to turbulence dissipation and particle injection are strong, adding to the nonlinear nature of efficient DSA. Describing the turbulence damping in a parameterized way, we reach two important results: first, for conditions typical of supernova remnant shocks, even a small amount of dissipated turbulence energy ($\sim 10\%$) is sufficient to significantly heat the precursor plasma, and second, the heating upstream of the shock leads to an increase in the injection of thermal particles at the sub-shock by a factor of several. In our results, the response of the non-linear shock

structure to the boost in particle injection prevented the efficiency of particle acceleration and magnetic field amplification from increasing. We argue, however, that more advanced (possibly, non-resonant) models of turbulence generation and dissipation may lead to a scenario in which particle injection boost due to turbulence dissipation results in more efficient acceleration and even stronger amplified magnetic fields than without the dissipation.

Subject headings: acceleration of particles – cosmic rays – supernova remnants – magnetic fields – turbulence – shock waves

1. Introduction

Observations of young supernova remnants (SNRs) suggest that strong collisionless shocks can simultaneously place a large fraction of the shock ram kinetic energy into relativistic protons (e.g., Blandford & Eichler 1987; Malkov & Drury 2001; Warren et al. 2005) and amplify the ambient turbulent magnetic field by large factors (e.g., Cowsik & Sarkar 1980; Reynolds & Ellison 1992; Bamba et al. 2003; Berezhko et al. 2003; Vink & Laming 2003; Uchiyama & Aharonian 2008). This coupling of diffusive shock acceleration (DSA) and magnetic field amplification (MFA) is critically important because the self-generated magnetic field largely determines the efficiency of DSA, the maximum particle energy a given shock can produce, and the synchrotron emission from radiating electrons.

The generation and dissipation of strong MHD turbulence in collisionless, multi-fluid plasmas is a complex process. Different nonlinear approaches to the modeling of the large scale structure of a shock undergoing efficient cosmic ray acceleration (e.g., McKenzie & Voelk 1982; Achterberg & Blandford 1986; Bell & Lucek 2001; Amato & Blasi 2006; Vladimirov et al. 2006; Pelletier et al. 2006; Zirakashvili et al. 2008) have predicted the presence of strong MHD turbulence in the shock precursor. However, an exact modeling of the shock structure in a turbulent medium, including nonthermal particle injection and acceleration, requires a nonperturbative, self-consistent description of a multi-component and multi-scale system including the strong MHD-turbulence dynamics. While a number of analytic models describing resonant and non-resonant amplification and damping of magnetic fluctuations have been proposed, these generally rely on the quasi-linear approximation that the fluctuations are small compared to the background magnetic field, i.e., $\Delta B \ll B_0$ (e.g., Wentzel 1974; Bykov & Toptygin 2005; Kulsrud 2005). No consistent analytic description of magnetic turbulence generation with $\Delta B \gtrsim B_0$ exists. For these reasons, numerical models with varying ranges of applicability have been proposed which offer a compromise between completeness and speed (e.g., Bell 2004; Amato & Blasi 2006; Vladimirov et al. 2006; Zirakashvili et al.

2008).

In principle, the problem can be solved completely with few assumptions and approximations with particle-in-cell (PIC) simulations (e.g., Bell 2004; Spitkovsky 2008; Niemiec et al. 2008) or, in the assumption that electrons are not dynamically important, by hybrid models (e.g., Winske & Omid 1996; Giacalone 2004). However, modeling the nonlinear generation of relativistic particles and strong magnetic turbulence in collisionless shocks is computationally challenging and PIC simulations will not be able to fully address this problem in nonrelativistic shocks for some years to come even though they can provide critical information on the plasma processes producing injection that can be obtained in no other way. In Appendix A we outline the requirements that a PIC simulation must fulfill in order to tackle the problem of efficient DSA with non-linear MFA in SNR shocks.

In the Monte Carlo approximation we use here, the plasma interactions are parameterized allowing us to study coupled nonlinear effects between the extended shock precursor and the gas subshock. In particular, we investigate the nonlinear effects caused by upstream plasma heating due to magnetic field dissipation.

The importance of the dissipation of turbulence in the shock precursor can be illustrated by the following estimate. Suppose that in a shock wave of speed u_0 , the turbulence is generated by the resonant cosmic ray (CR) streaming instability, so the energy density of the turbulence, U_w , evolves approximately as $u_0 dU_w(x)/dx = v_A dP_{\text{cr}}(x)/dx$ (e.g., Bell & Lucek 2001), where $P_{\text{cr}}(x)$ is the CR pressure at position x and v_A is the Alfvén speed. Ignoring all non-linear effects, the turbulence energy density at the shock positioned at $x = 0$ is $U_w(0) = \rho_0 u_0 v_{A0} \cdot P_{\text{cr}}(0)/(\rho_0 u_0^2)$. The ratio $\mathcal{E}_{\text{cr}} = P_{\text{cr}}(0)/(\rho_0 u_0^2)$ characterizes the efficiency of acceleration and is typically assumed to be on the order of ten percent or more. In the above, ρ is the fluid density and the subscript “0” always indicates far upstream values. Suppose a fraction, α_H , of this energy goes into heating of the thermal gas in the shock precursor so the energy density of the thermal plasma increases by $\Delta U_H(0) = \alpha_H U_w(0)$ at $x = 0$. Comparing $\Delta U_H(0)$ with the internal energy density of the far upstream plasma, ϵ_0 , we find

$$\eta_H = \frac{\Delta U_H(0)}{\epsilon_0} \approx \alpha_H \mathcal{E}_{\text{cr}} \frac{M_s^2}{M_A}, \quad (1)$$

where M_s is the sonic, and M_A the Alfvén, Mach number. If η_H is large, the thermal gas in the shock precursor is strongly heated and this influences the subshock strength and the particle injection efficiency. In a non-linearly modified shock, a change in the injection efficiency causes the whole shock structure to change. For typical supernova remnant (SNR) parameters (e.g., $u_0 \sim 3000 \text{ km s}^{-1}$, $T_0 \sim 10^4 \text{ K}$, $n_0 \sim 0.3 \text{ cm}^{-3}$, and $B_0 \sim 3 \text{ } \mu\text{G}$), the ratio $M_s^2/M_A \approx 250$, and values of α_H as low as a few to ten percent may be important.

Because existing analytical descriptions of MHD wave damping rely on the quasi-linear

approximation $\Delta B \ll B_0$, which is inapplicable for strong turbulence, and because an exact description of this process in the framework of non-linear DSA is currently impossible (see Appendix A), we propose a parameterization of the turbulence damping rate. In doing this, we are pursuing two goals. First, we make some predictions connecting cosmic ray spectra, turbulent magnetic fields and plasma temperatures, which, in principle, can be tested against high resolution X-ray observations in order to estimate the heating of the thermal gas by turbulence dissipation. And second, once heating is included in our simulation in a parameterized fashion, we will be ready to implement more realistic models of turbulence generation and dissipation as they are developed.

Our Monte Carlo simulation can be briefly summarized as follows (see Ellison et al. 1990a; Jones & Ellison 1991; Vladimirov et al. 2006, and references therein for more complete details). We describe particle transport in a plane shock by Bohm diffusion in a plasma flowing in the x -direction with speed $u(x)$. Particles move in small time steps as their local plasma frame momenta are ‘scattered’ at each step in a random walk process on a sphere in momentum space. Some shock heated thermal particles are injected into the acceleration process when their history of random scatterings in the downstream region takes them back upstream. These particles gain energy and some continue to be accelerated in the first-order Fermi mechanism. This form of injection is generally called ‘thermal leakage’ and was first used in the context of DSA in Ellison et al. (1981) (see also Ellison 1982).

The magnetic field determining the random walk properties through the diffusion coefficient is the ‘seed’ (interstellar) magnetic field after it has been amplified by a large factor by the CR streaming instability and compressed and advected downstream with the flow. The streaming instability in the non-linear regime ($\Delta B \gg B_0$) is described by the traditional quasi-linear equations, where the instability driving term is the CR pressure gradient. These quasi-linear equations are extrapolated into the non-linear regime in a parameterized fashion for lack of a more complete analytic description. The magnetic turbulence generated by the instability is assumed to dissipate at a rate proportional to the turbulence generation rate, and the dissipated energy is pumped directly into the thermal particle pool. An iterative scheme is employed to ensure the conservation of mass, momentum, and energy fluxes, thus producing a self-consistent solution of a steady-state, plane shock, with particle injection and acceleration coupled to the bulk plasma flow modification and to the magnetic field amplification and damping.

Our results show that even a small rate of turbulence dissipation can significantly increase the precursor temperature and that this, in turn, can increase the rate of injection of thermal particles. The nonlinear feedback of these changes on the shock structure, however, tend to cancel so that the spectrum of high energy particles is only modestly affected.

2. Model

The Monte Carlo simulation used here contains all of the elements of the code used in Vladimirov et al. (2006), and previously by Ellison and co-workers, i.e., it iteratively determines a self-consistent, steady-state shock solution with resonant magnetic field amplification. The present code, however, has been completely re-written and optimized for the problem of DSA with MFA in nonrelativistic, plane shocks. Besides including dissipation, the new code has been written for parallel processing and can model acceleration, in a reasonable time, to PeV energies¹. The particle transport is briefly described in Section 2.1, the amplification and dissipation of turbulence are described in Section 2.2, the effects of turbulence damping on the thermal plasma are described in Section 2.3, and the iterative procedure used to reach a self-consistent solution is given in Section 2.4.

2.1. Particle Transport and Injection in the Monte Carlo Code

Given a flow speed profile $u(x)$ and a diffusion coefficient $D(x, p)$ (which are obtained as explained below), the Monte Carlo code generates a thermal distribution of particles far upstream (or close to the shock, as described in Section 2.3 and Appendix B), and propagates them by small time steps, δt , scattering their momenta with the ‘pitch-angle scattering’ scheme described in detail in Ellison et al. (1990a). Since we assume strong turbulence ($\Delta B \gg B_0$), the concept of ‘pitch-angle’ as an angle measured with respect to the average magnetic field direction loses its meaning. Instead, we define the ‘pitch-angle’ as the angle that a particle’s plasma frame momentum makes with the direction of the bulk flow. Each scattering is elastic and isotropic in the local plasma frame, which moves at speed $u(x)$ with respect to the viscous subshock located at $x = 0$, and the angle of scattering is random, but its maximal value is determined by δt and by $D(x, p)$ (see Ellison et al. 1990a). When particles cross the subshock, or move in any compressive flow, the elastic scattering in the plasma frame makes them gain energy in the shock frame (see also Section B.1.1).

Injection of particles into the acceleration process occurs in the Monte Carlo simulation when a formerly thermal particle first crosses the viscous subshock backwards, i.e., going against the flow. The number of particles that do this, and the energy they gain, are determined only by the random particle histories; no parameterization of the injection process is

¹The ability of the Monte Carlo code to accelerate particles to PeV energies was shown in Ellison & Vladimirov (2008). The results we are interested in here do not require such high energies and we use a smaller dynamic range (see the note on dynamic range at the end of Section 3.2).

made other than the assumption of the diffusion coefficient value at various particle energies.²

Since microscopic plasma modeling of particle injection processes in non-relativistic subshocks with an appropriate 3-D PIC code is not yet available, all the models dealing with particle acceleration by shocks must assume some prescription of the injection process. We favor the present model for two reasons. First, our injection rate is set by the scattering prescription and doesn't require any additional assumptions. Second and even more important, our model was shown to agree well with spacecraft observations of the Earth's bow shock (Ellison & Moebius 1987; Ellison et al. 1990b), interplanetary shocks (Baring et al. 1997), and with 1-D hybrid PIC simulations (Ellison et al. 1993). We are aware of alternative models of particle injection, such as that used by Blasi et al. (2005), in which the shock is assumed transparent only to particles exceeding the thermal gyroradius by a certain factor. It is possible to simulate the injection with the Blasi et al. (2005) recipe in the Monte Carlo code, which was done by Ellison et al. (2005), but it should be noted that an injection threshold may be inconsistent with the bow shock observations reported in Ellison et al. (1990b). Our thermal injection model is also simultaneously consistent with the bow shock helium and CNO observations with no additional parameters or assumptions. A comparative analysis of the different injection recipes is beyond the scope of our present study.

A peculiarity of our approach is that in order to separate the CR particles from the thermal ones we use their history, and not their energy. By our definition, a thermal particle is one that we had introduced into the simulation upstream with a random thermal energy and that may have crossed the subshock going downstream, but has never crossed it back. Once a particle crosses the subshock (the coordinate $x = 0$, to be more precise) in the upstream direction, it by our definition is injected and becomes a CR particle (see also Appendix C).

As particles are propagated and scattered, their contributions to fluxes of mass, momentum, and energy are calculated at select positions. We also calculate the pressure produced by the thermal particles $P_{\text{th}}(x)$ and the spectrum of pressure of the CR particles $P_{\text{cr}}(x, p)$. (see details in Appendix B). The latter is related to the total CR pressure $P_{\text{cr}}(x)$ as

$$P_{\text{cr}}(x) = \int_0^{\infty} P_{\text{cr}}(x, p) dp , \quad (2)$$

and $P_{\text{cr}}(x, p)$ is then used to calculate the magnetic field amplification and dissipation, as

²As in previous implementations of our Monte Carlo model, the subshock is assumed to be transparent to all particles, including thermal ones, and possibly important plasma effects such as a cross-shock potential or large amplitude magnetic structures in the subshock layer are ignored.

described in Section 2.2.³

We assume in this paper that the acceleration is size-limited, and model the finite size of the shock with a free escape boundary (FEB), located at position $x_{\text{FEB}} < 0$ far upstream of the shock. All CR particles crossing the boundary escape freely from the system. The maximal particle momentum, p_{max} , is thus determined when the upstream diffusion length becomes comparable to $|x_{\text{FEB}}|$. For a spherical SNR blast wave, $|x_{\text{FEB}}|$ is on the order of the radius of the remnant.

2.2. Turbulence Amplification and Dissipation

We assume that far upstream there exists a uniform magnetic field, B_0 , parallel to the flow direction which is perturbed by transverse Alfvénic fluctuations with a power law energy spectrum. It is further assumed that these fluctuations produce Bohm diffusion for particles of all energies. Closer to the shock, where a population of accelerated particles drifting upstream is present, this seed turbulence is amplified by the CR streaming instability and additionally strengthened by the plasma compression. Once amplification begins, the spectrum of turbulence is no longer restricted to any particular form⁴. Assuming that the turbulence is described by the quantities $U_-(x, k)$ and $U_+(x, k)$ (k is the wavenumber of turbulence harmonics, U_- and U_+ are the spectra of energy density of structures propagating in the upstream and the downstream directions with respect to the thermal plasma, respectively), we model the evolution of the turbulence, as it is being advected with the plasma and amplified, with the following equations:

$$E_{\pm}[U] = (1 - \alpha_H)G_{\pm}[U] + I_{\pm}[U]. \quad (3)$$

³We note that notation has changed slightly from that used in Vladimirov et al. (2006). The subscript ‘tot’ indicating integral quantities has been eliminated, and these quantities are now denoted as $P_{\text{cr}}(x)$, $L(x)$, etc. The quantities representing spectral densities of pressure, flux, etc., are denoted with the same letters, but a different set of arguments: $P_{\text{cr}}(x, p)$, $L(x, k)$. To avoid ambiguity, explicit definitions relating the spectral densities to the integral densities are provided throughout the text. We also dropped the bar above the dissipation rate term $L(x)$ for simplicity.

⁴We assumed $U_{\pm} \propto k^{-1}$ for the seed turbulence. The choice of the seed turbulence spectrum does not significantly affect our results for two reasons. First, the diffusion coefficient assumed here only depends on the total power in the turbulence and is insensitive to the shape of the spectrum, and second, the rapidly growing fluctuations due to the streaming instability quickly overpower the seed spectrum. Despite our using the Bohm diffusion coefficient, we still keep track of the turbulence spectrum in the simulation since this will be used in future work where the diffusion coefficient is determined self-consistently from the wave spectrum.

Here, for readability, we abbreviated as E the evolution operator, as G the growth operator and as I the wave-wave interactions operator, acting on the spectrum of turbulence energy density $U = \{U_-(x, k), U_+(x, k)\}$. These quantities are defined as follows:

$$E_{\pm}[U] = (u \pm V_G) \frac{\partial}{\partial x} U_{\pm} + U_{\pm} \frac{d}{dx} \left(\frac{3}{2} u \pm V_G \right), \quad (4)$$

$$G_{\pm}[U] = \mp \frac{U_{\pm}}{U_+ + U_-} V_G \times \frac{\partial P_{\text{cr}}(x, p)}{\partial x} \bigg| \frac{dp}{dk}, \quad (5)$$

$$I_{\pm}[U] = \pm \frac{V_G}{r_{g0}} (U_- - U_+). \quad (6)$$

Here and throughout the paper, $r_{g0} = m_p u_0 c / (e B_0)$ – the gyroradius of a particle with a plasma frame speed equal to u_0 in the far upstream magnetic field B_0 . The parameter α_H describes the turbulence dissipation rate, and for $\alpha_H = 0$, equation (3) is exactly what was used in Vladimirov et al. (2006), except there it was assumed that $V_G \ll u(x)$. Keeping V_G relative to $u(x)$ results in a slightly greater amplification of magnetic field. In this system $u = u(x)$ is the flow speed and $V_G = V_G(x)$ is the parameter defining the turbulence growth rate and the wave speed⁵.

For simplicity, we assume $V_G(x) = B_0 / \sqrt{4\pi\rho(x)}$, in the present work, corresponding to $f_{\text{Alf}} = 0$ in Vladimirov et al. (2006), and emphasize that the use of equation (3) to describe the streaming instability when $\Delta B \gtrsim B_0$ is only a parameterization.

The growth operator G , which describes the turbulence amplification by the CR streaming instability, is proportional to the gradient of $P_{\text{cr}}(x, p)$, the latter being the spectrum of pressure of the CR particles driving the instability. $P_{\text{cr}}(x, p)$ is computed in the Monte Carlo simulation from the trajectories of particles, and the momentum p at which it is taken in (3) is the momentum resonant with the turbulent structures with wavenumber k . The resonance condition assumed is

$$k \frac{cp}{eB_0} = 1. \quad (7)$$

⁵As explained in Vladimirov et al. (2006), in the quasilinear case, $\Delta B \ll B_0$, the wave speed and the speed determining turbulence growth rate are both equal to the Alfvén speed, $V_G(x) = v_A = B_0 / \sqrt{4\pi\rho(x)}$. In the case of strong turbulence, $\Delta B \gtrsim B_0$, we hypothesise that the resonant streaming instability can still be described by equations (3) with V_G being a free parameter ranging from $B_0 / \sqrt{4\pi\rho(x)}$ to $B_{\text{eff}} / \sqrt{4\pi\rho(x)}$.

The parameter α_H enters the equations of turbulence evolution (3) through the factor $(1 - \alpha_H)$, by which the term G describing the magnetic field amplification by the CR streaming is reduced (it is assumed that $0 \leq \alpha_H \leq 1$). By writing this, we assumed simply that at all wavelengths only a fraction $(1 - \alpha_H)$ of the instability growth rate goes into the magnetic turbulence, and the remaining fraction α_H is lost in the dissipation process. The factor $(1 - \alpha_H)$ in (3) can also be understood in the following way: Vladimirov et al. (2006) derived their equations (11) and (12) from equation (3) by assuming that the loss term $L = 0$ (L here is \bar{L} in their notation), but now we are assuming that

$$L = -\alpha_H \cdot v_{a,x} \frac{\partial P_{\text{cr}}}{\partial x}. \quad (8)$$

For $\alpha_H = 0$ no dissipation occurs, and the CR streaming instability pumps the energy of the accelerated particles into the magnetic turbulence, amplifying the effective magnetic field most efficiently. For $\alpha_H = 1$ the additional turbulence energy produced by the instability is assumed to immediately dissipate, and the scattering in the shock is assumed to be provided only by the seed turbulence slightly increased by the plasma compression.

The energy dissipation rate at all wavelengths is then

$$L(x) = \int_0^\infty L(x, k) dk = \alpha_H \cdot V_G \frac{dP_{\text{cr}}(x)}{dx}, \quad (9)$$

and we assume that all this energy goes directly into heating thermal particles. The modeling of the thermal plasma heating is covered in detail in Section 2.3.

When equation (3) is solved, the resulting $U_\pm(x, k)$ are used to calculate the amplified effective magnetic field

$$B_{\text{eff}}(x) = \left[4\pi \int_0^\infty U_-(x, k) dk + 4\pi \int_0^\infty U_+(x, k) dk \right]^{1/2}, \quad (10)$$

the turbulence pressure

$$P_w(x) = \frac{B_{\text{eff}}^2(x)}{8\pi} \quad (11)$$

and the turbulence energy flux

$$F_w(x) = \left(\frac{3}{2}u - V_G \right) \int_0^\infty U_-(x, k) dk +$$

$$\left(\frac{3}{2}u + V_G\right) \int_0^\infty U_+(x, k) dk \quad (12)$$

(see equations (15), (18) and (19) in Vladimirov et al. (2006)), which are then used in the derivation of a self-consistent solution, as discussed in Section 2.4 below. In the present paper we do not neglect V_G in the sum with u , which results in a slightly lower compression ratio r_{tot} than in the case $3/2u \pm V_G \approx 3/2u$, that was adopted in Vladimirov et al. (2006).

As mentioned by Caprioli et al. (2008), effects from the transmission and reflection of Alfvén waves at the subshock could be important, and accounting for these effects may further lower the compression ratio r_{tot} . We do not account for reflection and linear transformations of Alfvén waves to other MHD modes (magnetosonic, entropy, etc.) at the subshock (see McKenzie and Westphal 1970) in the present paper, because a correct description of these effects on the subshock in highly turbulent media must contain simultaneously some other comparable effects. Indeed, MHD waves interacting with a shock produce stochastic ripples in the shock surface and these ripples produce an effective broadening of the shock spatial structure determined by the turbulence spectrum (see Bykov 1982). Moreover, as we argue in Appendix C, accounting for suprathermal particles modifies the standard Rankine-Hugoniot relations at the subshock and these effects could make it impossible to identify the subshock as a plane discontinuity, as assumed in all existing semi-analytic models. Clearly, these phenomena are important and require further investigation but they are beyond the scope of our simplified description of MFA. Nevertheless, we believe our predictions regarding the turbulence dissipation in the shock precursor are qualitatively correct.

2.3. Heating of Thermal Plasma

Repeating the derivation of equation (9) in McKenzie & Voelk (1982), one obtains for a steady-state shock:

$$\frac{u\rho^\gamma}{\gamma - 1} \frac{d}{dx} (P_{\text{th}}\rho^{-\gamma}) = L(x) . \quad (13)$$

Here and elsewhere, $\rho = \rho(x)$, $u = u(x)$, and $P_{\text{th}} = P_{\text{th}}(x)$. The quantity $L(x)$ is the dissipation rate defined in (9), and the ratio of specific heats of an ideal nonrelativistic gas is $\gamma = 5/3$. For $L(x) = 0$, equation (13) reduces to the adiabatic heating law, $P_{\text{th}} \sim \rho^\gamma$ and, for a non-zero $L(x)$, it describes the heating of the thermal plasma in the shock precursor due to the dissipation of magnetic turbulence. The fluid description of heating given by equation (13), while it doesn't include details of individual particle scattering, can be used in the Monte Carlo simulation to replace particle scattering and determine heating in the

shock precursor. This merging of analytic and Monte Carlo techniques, or Analytic Precursor Approximation (APA), is described in detail in Appendix B.

The APA only affects our treatment of thermal (i.e., not injected) particles in the precursor and involves two steps. The first is to introduce thermal particles into the simulation, not far upstream as we did before, but at some position $x_{\text{APA}} < 0$ close to the subshock and with a temperature equal to what Eq. (13) and the ideal gas law suggest:

$$T(x) = \frac{P_{\text{th}}(x)}{k_B n_0 (u_0/u(x))}, \quad (14)$$

where all quantities are taken at $x = x_{\text{APA}}$ and P_{th} is calculated from (13) (n_0 and u_0 are the far upstream number density and shock speed, and k_B is Boltzmann’s constant). The second step is to calculate the thermal gas pressure throughout the precursor (at $x < x_{\text{APA}}$) using (13) instead of tracing particle motions.

The main effects of turbulence dissipation in our model are: (i) a decrease in the value of the amplified field $B_{\text{eff}}(x)$, which determines the diffusion coefficient, $D(x, p)$; (ii) an increase in the temperature of particles just upstream of the subshock, which influences the injection of particles into the acceleration process, and (iii) an increase in the thermal particle pressure $P_{\text{th}}(x < 0)$, and a decrease in the turbulence pressure $P_w(x)$, which enter the conservation equations described in Section 2.4. Since all of these processes are coupled, a change in dissipation influences the overall structure of the shock.

2.4. Closure of the Model

Typically, we begin our simulation by propagating particles, with a pre-set diffusion coefficient $D(x, p)$, in an unmodified shock, where the flow speed jumps discontinuously from u_0 to u_2 , that is, $u(x) = u_0$ for $x < 0$ and $u(x) = u_2$ for $x > 0$.⁶ This allows us to calculate the various fluxes and other quantities, such as the CR pressure spectrum $P_{\text{cr}}(x, p)$, at any position x . The latter is used to solve Eq. (3), which yields the turbulence spectra $U_{\pm}(x, k)$ and, subsequently, the amplified effective field $B_{\text{eff}}(x)$ and the pressure of the magnetic turbulence $P_w(x)$. The spectrum $P_{\text{cr}}(x, p)$ also provides the turbulence dissipation rate (9) and the resulting pressure of the turbulence-heated gas (13).

⁶Everywhere in the text, unless otherwise noted, the subscript ‘0’ indicates a far upstream value, ‘1’ indicates a value just upstream of the subshock, and ‘2’ indicates a downstream value. For example, $u_0 = u(x = -\infty)$, $u_1 = u(x_{\text{tr}})$, and $u_2 = u(x > 0)$. See Appendix B.1.1 for definition of x_{tr} .

The equations for the conservation of mass and momentum fluxes are:

$$\rho(x)u(x) = \rho_0 u_0 \quad (15)$$

(ρ and u are the mass density and the flow speed) and

$$\Phi_P(x) = \Phi_{P0}, \quad (16)$$

where $\Phi_P(x)$ is the flux of the x -component of momentum in the x -direction including the contributions from particles and turbulence, and Φ_{P0} is the far upstream value of momentum flux, i.e.,

$$\Phi_{P0} = \rho_0 u_0^2 + P_{th0} + P_{w0} . \quad (17)$$

The quantity Φ_P is defined as

$$\Phi_P(x) = \int p_x v_x f(x, \mathbf{p}) d^3 p + P_w(x), \quad (18)$$

(here p_x and v_x are the x -components of momentum and velocity of particles, and $f(\mathbf{p})$ is their distribution function, all measured in the shock frame), and in the simulation it is calculated by summing the contributions of the particles crossing a grid location and adding the turbulence pressure P_w defined in (11). See details of this computation in Appendix B.

Initially, in our simulation, the shock doesn't have a self-consistent structure because we start with an unmodified shock and $\Phi_P(x)$ is overestimated at all locations where accelerated particles are present. The next step is to use the calculated macroscopic quantities to find a new $u(x)$ that reduces the mismatch between the local momentum flux and the far upstream value of it Φ_{P0} for $x < 0$. We do this by calculating

$$u'(x) = u(x) + s \cdot \frac{\Phi_P(x) - \Phi_{P0}}{\rho_0 u_0}, \quad (19)$$

where $u'(x)$ is the predicted flow speed for the next iteration, and s is a small positive number (typically around 0.1), characterizing the pace of the iterative procedure. At this point we also refine our estimate for the particle diffusion coefficient which, as in Vladimirov et al. (2006), is assumed to be Bohm diffusion such that the particle mean free path is equal to its gyroradius in the effective, amplified field $B_{\text{eff}}(x)$:

$$D(x, p) = \frac{v\lambda}{3} = \frac{vcp}{3eB_{\text{eff}}(x)}, \quad (20)$$

where $B_{\text{eff}}(x)$ is defined in (10).

The predicted $u(x)$ and $D(x, p)$ are then used in a new iteration where particles are injected and propagated. The calculated CR pressure, momentum flux, etc. are then used

to refine the guesses for $u(x)$ and $D(x, p)$ for the next iteration, and so on. This procedure is continued until all quantities converge.

In order to conserve momentum and energy, the compression ratio, $r_{\text{tot}} = u_0/u_2$, must be determined self-consistently with the shock structure. To determine r_{tot} we use the condition of the conservation of energy flux given by:

$$\Phi_E(x) + Q_{\text{esc}}(x) = \Phi_{E0}, \quad (21)$$

where $\Phi_E(x)$ is the energy flux of particles and turbulence in the x -direction, Q_{esc} is the energy flux of escaping particles at the FEB,⁷ and the far upstream value of the energy flux is

$$\Phi_{E0} = \frac{1}{2}\rho_0 u_0^3 + \frac{\gamma}{\gamma - 1} P_{\text{th}0} u_0 + F_{w0}. \quad (22)$$

The quantity $\Phi_E(x)$ is defined as

$$\Phi_E(x) = \int K v_x f(x, \mathbf{p}) d^3 p + F_w(x), \quad (23)$$

K being the kinetic energy of a particle with momentum p measured in the shock frame, and F_w is the energy flux of the turbulence defined in (12). The details of calculating $\Phi_E(x)$ in the simulation are given in Appendix B, and the explanation of how $\Phi_E(x)$ is used in an iterative procedure converging to a consistent r_{tot} is given in Appendix D.

3. Results

3.1. Particle Injection in Unmodified Shocks (Subshock Modeling)

In order to isolate the effects of plasma heating on particle injection, we first show results for unmodified shocks, i.e., $u(x < 0) = u_0$ and $u(x > 0) = u_0/r_{\text{tot}}$, with fixed r_{tot} . In these models particle acceleration, magnetic field amplification and turbulence damping are included consistently with each other, but we do not obtain fully self-consistent solutions conserving momentum and energy, since this requires the shock to be smoothed, while we intentionally fix $u(x)$.

⁷Particle escape at an upstream FEB also causes the mass and momentum fluxes to change but these changes are negligible as long as $u_0 \ll c$ (Ellison 1985).

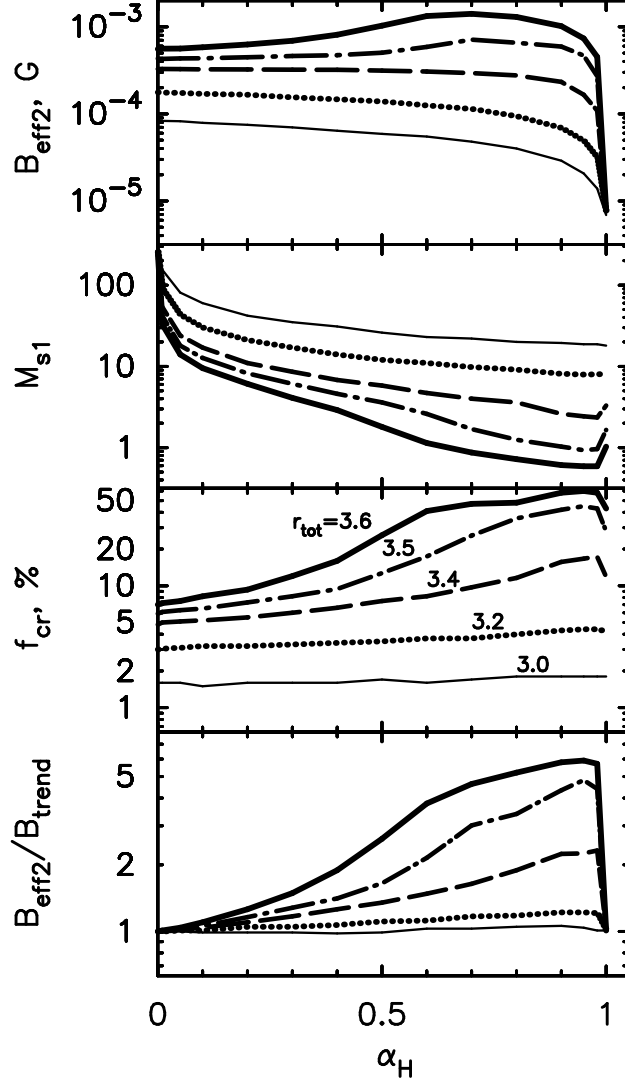


Fig. 1.— Dependence of magnetic field amplification and particle injection on the rate of magnetic turbulence dissipation in unmodified shocks. Results for shocks with compression ratios $r_{\text{tot}}=3.0, 3.2, 3.4, 3.5$ and 3.6 are represented by the thin solid, dotted, dashed, dash-dotted and thick solid lines, respectively. The x -axis variable is the turbulence dissipation rate α_H (constant throughout a shock), and the plotted quantities are the amplified downstream effective magnetic field B_{eff2} , the subshock sonic Mach number M_{s1} , the fraction of simulation particles injected into the acceleration process f_{cr} , and the ratio of amplified field to B_{trend} downstream from the shock.

In Fig. 1 we show results where the compression ratio is varied between $r_{\text{tot}} = 3$ and 3.6 as indicated. In all models, $u_0 = 3000 \text{ km s}^{-1}$, $T_0 = 10^4 \text{ K}$, $n_0 = 0.3 \text{ cm}^{-3}$ and $B_0 = 3 \mu\text{G}$ (the corresponding sonic and Alfvén Mach numbers are $M_{s0} \approx M_{A0} \approx 250$). The FEB was set at $x_{\text{FEB}} = -3 \cdot 10^4 r_{g0}$ (our spatial scale unit $r_{g0} = m_p u_0 c / (e B_0)$), and for each r_{tot} we obtained results for different values of α_H between 0 and 1. The values plotted in the top three panels of Fig. 1 are the amplified magnetic field downstream, B_{eff2} , the Mach number right before the shock, M_{s1} (this is not equal to M_{s0} because of the plasma heating due to turbulence dissipation), and the fraction of thermal particles in the simulation that crossed the shock in the upstream direction at least once (i.e., got injected), f_{cr} . The bottom panel shows the ratio of the calculated downstream effective magnetic field B_{eff2} to trend values $B_{\text{trend}}(\alpha_H)$; what is meant by “trend” is explained below.

Looking at the curve for B_{eff2} in the $r_{\text{tot}} = 3.0$ model, one sees an easy to explain behavior: as the magnetic turbulence dissipation rate increases, the value of the amplified magnetic field decreases, going down to $B_0 r_{\text{tot}}^{3/4}$ (the upstream field compressed at the shock) for $\alpha_H = 1$. Increasing α_H simply causes more energy to be removed from magnetic turbulence and put into thermal particles, thus decreasing the value of B_{eff2} .⁸ In our model, the amount of dissipated turbulence energy scales linearly with α_H . Therefore, the trend of B_{eff2} changing with α_H under the assumption that the total efficiency of the streaming instability is unchanged, but the energy is channelled from magnetic turbulence to thermal particles, can be described as

$$B_{\text{trend}}^2(\alpha_H) = \left(B_0 r_{\text{tot}}^{3/4} \right)^2 + (1 - \alpha_H) \times \left[B_{\text{eff2}}^2 \Big|_{\alpha_H=0} - \left(B_0 r_{\text{tot}}^{3/4} \right)^2 \right], \quad (24)$$

where the first term on the right hand side is the B_0 compressed at the shock (the compression factor $r_{\text{tot}}^{3/4}$ is explained by equation (13) in Vladimirov et al. 2006), and the second term is proportional to the amount of the magnetic turbulence energy density generated by the instability for $\alpha_H = 0$, reduced by the factor $(1 - \alpha_H)$. Neglecting B_0 , Eq. (24) predicts $B_{\text{trend}} \propto \sqrt{1 - \alpha_H}$. The comparison of B_{eff2} with $B_{\text{trend}}(\alpha_H)$ from (24) is shown in the bottom panel of Fig. 1. It is clear that the above trend matches the calculations very well for $r_{\text{tot}} = 3.0$. One also can see that the sonic Mach number in this simulation decreased from the upstream value of 250 to approximately 20, and that the fraction of injected particles remained almost constant as α_H was varied.

⁸We use this result, with well understood behavior, to test the implementation of turbulence dissipation in our simulation.

The curves for $r_{\text{tot}} = 3.2$ demonstrate the same behavior, and the shape of the B_{eff2} curve is similar to the one for $r_{\text{tot}} = 3.0$, with the higher compression ratio producing a higher value of the amplified magnetic field due to a greater number of particles getting injected. The calculated B_{eff2} deviates from the trend $B_{\text{trend}}(\alpha_H)$ more than in the $r_{\text{tot}} = 3.0$ case, and this deviation marks the emergence of an effect that becomes more pronounced as r_{tot} increases.

The plots for $r_{\text{tot}} \gtrsim 3.4$ present a qualitatively different behavior from those with $r_{\text{tot}} \lesssim 3.2$. The downstream magnetic field B_{eff2} does decrease with increasing α_H , but not as rapidly as in the previous two cases, and there is a switching point at $\alpha_H \approx 0.95$ in the curves for M_{s1} and f_{cr} . The bottom panel of Fig. 1 shows a deviation of B_{eff2} from the trend (24) by a large factor in the $r_{\text{tot}} = 3.4$ case. This effect becomes even more dramatic for $r_{\text{tot}} = 3.5$ and $r_{\text{tot}} = 3.6$ where B_{eff2} , contrary to expectations, increases with α_H before $\alpha_H \rightarrow 1$. The fact that the final energy in turbulence can increase as more energy is transferred from the turbulence to heat indicates the nonlinear behavior of the system and shows how sensitive the acceleration is to precursor heating.

Indeed, if the upstream plasma is not heated sufficiently (as in the $r_{\text{tot}} < 3.4$ cases), then the thermal particles first reaching the shock are cold ($T_1 \sim T_0$), and just upstream of the subshock the sonic Mach number M_{s1} has a large value (much greater than 10 for any α_H). As these thermal particles cross the shock, their momenta in the downstream plasma frame lie in a very narrow cone opening in the downstream direction, with the opening angle around $\theta \sim M_{\text{s1}}^{-1}$, making it equally difficult for most particles to turn around, cross the subshock backwards and get injected into the acceleration process. As long as θ is small (or M_{s1} is large enough), the number of injected particles is insensitive to the exact opening angle and f_{cr} stays relatively constant, as seen in the third panel of Fig. 1 for the $r_{\text{tot}} = 3.0$ case.

The injection rate increases with r_{tot} and for $r_{\text{tot}} = 3.6$, even with α_H as low as 0.1, the CR-generated turbulence heats the thermal plasma through dissipation enough to lower M_{s1} to ~ 10 . Increasing α_H further lowers M_{s1} even more, quickly increasing the probability that a downstream thermal particle will return upstream, thus boosting the injection rate (f_{cr} rapidly goes up with α_H in the $r_{\text{tot}} \geq 3.4$ cases). It turns out that this effect overcomes the reduction of B_{eff2} due to damping, and B_{eff2} starts increasing with α_H .

For any r_{tot} , at some high enough value of α_H (near 0.90), the decrease in magnetic turbulence due to dissipation dominates the increase in injection and the magnetic field drops. As $\alpha_H \rightarrow 1$, and B_{eff2} becomes small enough, the efficiency of particle acceleration reduces sufficiently to cut down the total energy put into magnetic turbulence and the corresponding fraction of this energy dissipated into the thermal particles. This causes M_{s1}

to turn up and f_{cr} to turn down at about $\alpha_H = 0.95$, as shown in the Fig. 1.

It is worth mentioning that the observed increase of particle injection due to the precursor plasma heating is a consequence of the thermal leakage model of particle injection adopted here. In this model, a downstream particle, thermal or otherwise, with plasma frame speed $v > u_2$, has a probability to return upstream which increases with v (see Bell 1978, for a discussion of the probability of returning particles). That is, we assume that the subshock is transparent to all particles with $v > u_2$, but only some of these particles get injected, depending on their random histories. Particles that don't get injected are convected far downstream out of the system. An alternative model of injection (see, for example, Blasi et al. 2005) is one where only particles with a gyroradius greater than the shock thickness can get injected. The assumption with this threshold injection model is that the subshock thickness is comparable to the gyroradius of a downstream thermal particle and only those particles with speeds $v > \xi v_{\text{th}}$ can be injected. Particles with $v < \xi v_{\text{th}}$ are somehow blocked by the subshock. Here, v_{th} is the downstream thermal speed and ξ is a free parameter, typically taken to be between 2 and 4.

Despite being similar, it can be expected that these injection models will react differently to precursor heating. Namely, in the Blasi et al. (2005) model the fraction of injected particles may be insensitive to the precursor heating if ξ is fixed⁹, because the same particle injection rate occurs regardless of the pre-subshock temperature T_1 and downstream temperature T_2 . While both models are highly simplified descriptions of the complex subshock (see, e.g. Malkov 1998; Giacalone & Ellison 2000), they offer two scenarios for grasping a qualitatively correct behavior of a shock where particle injection and acceleration are coupled to turbulence generation and flow modification. Hopefully, a clearer view of particle injection by self-generated turbulence in a strongly magnetized subshock will become available when relevant full particle PIC or hybrid simulations are performed.

With the general trends observed here in mind, we now show how nonlinear effects modify the effect dissipation has on injection and MFA.

⁹Amato & Blasi (2006), who performed a brief analysis of the impact of the turbulence dissipation on the nonlinear shock structure in a way similar to ours, did not report an influence of heating on the injection rate.

3.2. Fully Nonlinear Model

In this section we demonstrate the results of the fully nonlinear models, in which the flow structure, compression ratio, magnetic turbulence, and particle distribution are all determined self-consistently, so that the fluxes of mass, momentum and energy are conserved across the shock.

We use two sets of parameters, one with the far upstream gas temperature $T_0 = 10^4$ K and the far upstream particle density $n_0 = 0.3 \text{ cm}^{-3}$, typical of the cold interstellar medium (ISM), and one with $T_0 = 10^6$ K and $n_0 = 0.003 \text{ cm}^{-3}$, typical of the hot ISM. In both cases we assumed the shock speed $u_0 = 5000 \text{ km s}^{-1}$, and the initial magnetic field $B_0 = 3 \text{ } \mu\text{G}$ (giving an equipartition of magnetic and thermal energy far upstream, $n_0 k_B T_0 \approx B_0^2 / (8\pi)$). The corresponding sonic and Alfvén Mach numbers are $M_s \approx M_A \approx 400$ in both cases). The size of the shocks was limited by a FEB located at $x_{\text{FEB}} = -10^5 r_{g0} \approx -3 \cdot 10^{-4} \text{ pc}$. For both cases, we ran seven simulations with different values of the dissipation rate α_H , namely $\alpha_H \in \{0; 0.1; 0.25; 0.5; 0.75; 0.9; 1.0\}$. Also, for the hot ISM ($T_0 = 10^6$ K) case we ran a simulation neglecting the streaming instability effects, i.e., keeping the magnetic field constant throughout the shock and assuming that the precursor plasma is heated only by adiabatic compression (this model will be referred to as the ‘no MFA case’).

Table 1. Summary of Non-linear Simulation in a Cold ISM

α_H	0.00	0.10	0.25	0.50	0.75	0.95	1.00
r_{tot}	16.0	16.2	14.5	14.6	14.0	13.2	13.0
r_{sub}	2.95	2.83	2.75	2.59	2.50	2.50	2.51
$B_{\text{eff2}}, \mu\text{G}$	345	323	284	232	158	71	21
$B_{\text{trend}}, \mu\text{G}$	345	327	299	245	174	80	21
$\langle T(x < 0) \rangle, 10^4 \text{ K}$	1.06	4.3	9.0	17	26	37	56
$T_1, 10^4 \text{ K}$	3.3	68	160	330	490	610	650
$T_2, 10^4 \text{ K}$	1400	1500	1600	1600	1800	2000	2200
M_{s1}	44	9.5	6.3	4.2	3.5	3.3	3.2
$f_{\text{cr}}, \%$	1.0	1.2	1.6	2.1	2.6	3.1	3.2
$p_{\text{max}}/m_p c$	500	450	400	350	250	150	80
$\langle \gamma(x < 0) \rangle$	1.33	1.33	1.33	1.33	1.34	1.34	1.34
γ_2	1.38	1.38	1.38	1.39	1.39	1.40	1.41
$x_{\text{tr}}/r_{\text{g0}}$	-0.005	-0.001	-0.001	-0.001	-0.002	-0.004	-0.02
$x_{\text{APA}}/r_{\text{g0}}$	-0.04	-0.06	-0.06	-0.09	-0.23	-0.57	-2.1

Note. — Here α_H , the fraction of dissipated energy, is the model input parameter, and the rest are results of the self-consistent simulation, as follows: $r_{\text{tot}} = u_0/u_2$ is the total shock compression ratio, $r_{\text{sub}} = u_1/u_2$ is the subshock compression, B_{eff2} is the amplified effective magnetic field downstream, B_{trend} is the trend value calculated from Eq. (24), $\langle T(x < 0) \rangle$ is the temperature of the precursor averaged over the volume from $x = x_{\text{FEB}}$ to $x = 0$, T_1 is the temperature at $x = x_{\text{tr}}$, T_2 is the volume-averaged temperature at $x > 0$ (all temperatures are calculated from the ideal gas law (14)), M_{s1} is the sonic Mach number at $x = x_{\text{tr}}$, f_{cr} is the fraction of injected thermal particles, p_{max} is the maximum particle momentum (i.e., the momentum at which $f(p)$ starts falling off exponentially with p), $\langle \gamma(x < 0) \rangle$ is the value of the polytropic index of particle gas, calculated from particle pressure and internal energy density as described in Appendix D, and averaged over volume from $x = x_{\text{FEB}}$ to $x = 0$, γ_2 is the same quantity averaged over $x > 0$, x_{tr} is the point at which the subshock starts, as defined by Eq. (B4), and x_{APA} is the point defined by Eq. (B11), at which thermal particles were introduced by the APA procedure as described in Appendix B.

Table 2. Summary of Non-linear Simulation in a Hot ISM

α_H	0.00	0.10	0.25	0.50	0.75	0.95	1.00	No MFA
r_{tot}	8.1	8.2	8.3	8.0	7.8	7.4	7.3	13
r_{sub}	2.92	2.75	2.55	2.44	2.22	2.15	2.12	2.75
$B_{\text{eff2}}, \mu\text{G}$	62	60	55	44	32	17	14	21
$B_{\text{trend}}, \mu\text{G}$	62	59	54	45	33	19	13	-
$\langle T(x < 0) \rangle, 10^6 \text{ K}$	1.04	1.3	1.7	2.3	3.1	3.9	4.2	1.1
$T_1, 10^6 \text{ K}$	2.0	6.0	13	23	34	42	43	2.7
$T_2, 10^6 \text{ K}$	53	49	47	55	62	72	75	22
M_{s1}	10.9	5.8	3.7	2.6	2.1	1.9	1.9	4.7
$f_{\text{cr}}, \%$	1.2	1.6	2.5	4.0	6.4	6.9	6.4	2.4
$p_{\text{max}}/m_p c$	150	120	110	100	90	70	60	80
$\langle \gamma(x < 0) \rangle$	1.34	1.34	1.34	1.34	1.34	1.34	1.35	1.34
γ_2	1.43	1.43	1.43	1.44	1.45	1.45	1.45	1.41
$x_{\text{tr}}/r_{\text{g0}}$	-0.04	-0.02	-0.02	-0.02	-0.03	-0.07	-0.05	-0.02
$x_{\text{APA}}/r_{\text{g0}}$	-0.1	-0.1	-0.2	-0.2	-0.4	-0.9	-1.4	-0.1

Note. — See the note for Table 1 for the explanation of listed quantities.

Referring to Tables 1 and 2, we summarize some of the results of these models. The effect of the turbulence dissipation into the thermal plasma is evident in the values of the pre-subshock temperature T_1 , the downstream temperature T_2 , and the volume-averaged precursor temperature $\langle T(x < 0) \rangle$ (the averaging takes place between $x = x_{\text{FEB}}$ and $x = 0$). The temperatures were calculated from the thermal particle pressure $P_{\text{th}}(x)$ using the ideal gas law equation (14). The value of T_1 depends drastically on the level of the turbulence dissipation α_H , increasing from $\alpha_H = 0$ to $\alpha_H = 0.5$ by a factor of 100 in the cold ISM case, and by a factor of 11 in the hot ISM case (less in the latter case, because the efficiency of the CR streaming instability in generating the magnetic turbulence is less for the smaller M_s and M_A for $T = 10^6$ K). The values of the temperature as high as T_1 are achieved upstream only near the subshock; the volume-averaged upstream temperature, $\langle T(x < 0) \rangle$, is significantly lower. The factors by which $\langle T(x < 0) \rangle$ increases in the above cases are 17 and 2.3, respectively. The value of M_{s0}^2/M_{A0} is large in our models, and the estimate (1) predicts that even a small amount of dissipation is enough to raise the precursor temperature significantly. This is confirmed by our results: even $\alpha_H = 0.1$ is enough to raise the pre-subshock temperature T_1 approximately 20 times in the cold ISM ($T_0 = 10^4$ K) case.

The downstream temperature, T_2 , varies less with changing α_H , because it is largely determined by the compression at the subshock, which is controlled by many factors as we discuss below. It is worth mentioning the case without MFA reported in Table 2. Besides having a much larger compression factor than the shocks with MFA ($r_{\text{tot}} = 18$ as opposed to $r_{\text{tot}} \lesssim 8$), it has a much smaller downstream temperature ($T_2 = 1.2 \cdot 10^7$ K as opposed to $T_2 \gtrsim 5.3 \cdot 10^7$ K). These effects of dissipation on the precursor temperature may be observable.

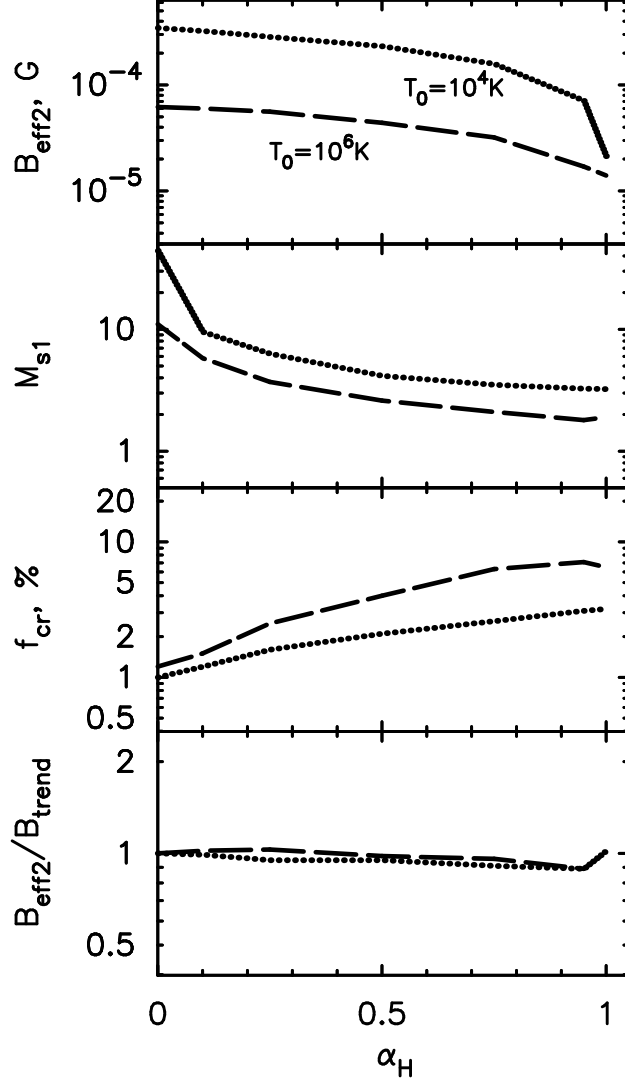


Fig. 2.— Dependence of particle injection and magnetic field amplification on the rate of magnetic turbulence dissipation in the non-linearly modified shock with $u = 5000 \text{ km s}^{-1}$ in the cold ISM and the hot ISM cases (the fully self-consistent models). The x -axis variable is the turbulence dissipation rate α_H (constant throughout a shock), and the plotted quantities are the amplified downstream effective magnetic field B_{eff2} , the subshock sonic Mach number M_{s1} , the fraction of simulation particles injected into the acceleration process f_{cr} , and the ratio of amplified field to B_{trend} downstream from the shock.

In Figure 2 we show results for f_{cr} , M_{s1} , B_{eff2} , and B_{trend} which can be compared to the results for unmodified shocks shown in Figure 2. For the modified shocks, the fraction of the thermal particles crossing the shock backwards for the first time, f_{cr} , clearly increases by a large factor with α_H , which can be explained by the value of M_{s1} dropping quickly below 10. One could expect that the amplified effective magnetic field B_{eff2} would behave similarly to the $r_{\text{tot}} = 3.5$ case in Section 3.1, i.e. that B_{eff2} would not decrease or even would increase for larger α_H . Instead, B_{eff2} behaves approximately according to the trend (24), as the values of B_{trend} from Tables 1 and 2 show and the bottom panel of Fig. 2 illustrates. The important point is that, even though precursor heating causes the *injection efficiency* to increase substantially, the *efficiency of particle acceleration* and magnetic turbulence generation is hardly changed. We base this assertion on the fact that B_{eff2} remains close to B_{trend} , which was derived under the assumption that changing α_H preserves the total energy generated by the instability, but re-distributes it between the turbulence and the thermal particles. The fact that the particle acceleration efficiency is insensitive to α_H is directly seen in the results displayed in Figure 5 below.

Considering how much the injection rate f_{cr} increases with α_H , and how much the upstream temperature of the thermal plasma, T_1 , is affected by the heating, it is somewhat surprising that the trend of the amplified effective field B_{eff2} is unaffected. The mechanism by which the shock adjusts to the changing heating and injection in order to preserve the MFA efficiency can be understood by looking at the trend of the total compression ratio r_{tot} and the subshock compression ratio r_{sub} in Tables 1 and 2: they both decrease significantly for higher α_H . The decrease in r_{sub} is easy to understand: with the turbulence dissipation operating in the precursor M_{s1} goes down, which lowers r_{sub} . Additionally, decreasing P_{w1} helps to reduce r_{sub} , and with a boost of the particle injection rate, the particles returning for the first time increase in number and build up some extra pressure just upstream of the shock, which causes the flow to slow down in that region, thus reducing the ratio r_{sub} . The decrease in r_{tot} results from more complex processes. Here, the histories of ‘adolescent’ particles, i.e., those particles returning upstream for the first time or for the first few times, are critical. Adolescent particles, while superthermal, are still highly anisotropic in the shock frame and how they get accelerated in the smoothed precursor just upstream of the subshock determines the number and energies of the ‘mature’ superthermal particles, i.e., those particles with enough energy to be nearly isotropic in the shock frame. The mature particles determine the CR pressure and precursor smoothing on larger scales.

Further understanding of the shock adjustment to the changing dissipation can be gained by studying Figures 3 - 5, in which we plot the spatial structure and the momentum-dependent quantities of the shocks in the cold ISM and the hot ISM cases for $\alpha_H \in \{0; 0.5; 1\}$.

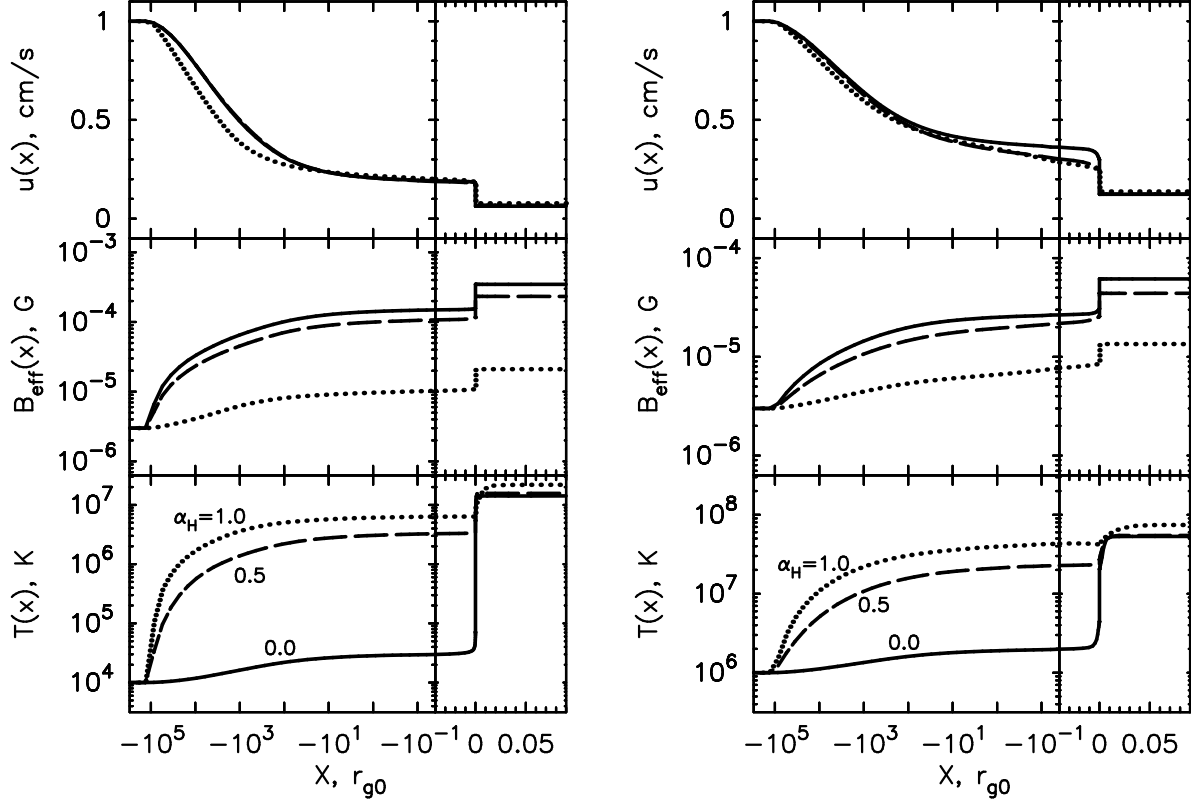


Fig. 3.— Results of non-linear simulations in the cold ISM (left) and hot ISM (right) with different values of α_H . The solid, dashed and dotted lines correspond, respectively, to $\alpha_H = 0, 0.5$ and 1.0 . The plotted quantities are the bulk flow speed $u(x)$, the effective amplified magnetic field $B_{\text{eff}}(x)$ and the thermal gas temperature $T(x)$. The shock is located at $x = 0$, and note the change from the logarithmic to the linear scale at $x = -0.05 r_{g0}$.

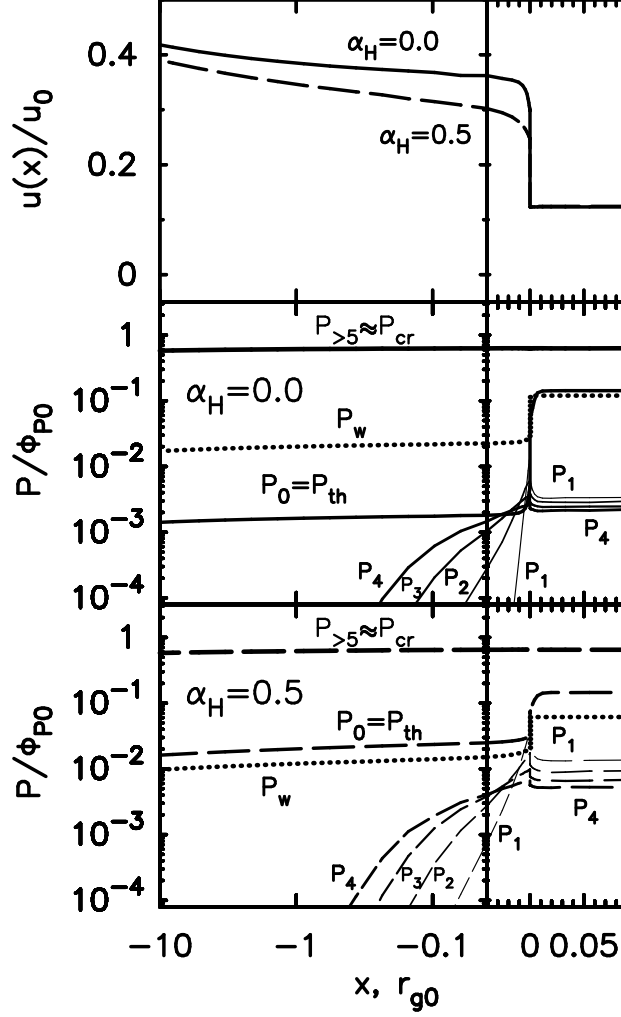


Fig. 4.— Enlarged subshock region in the hot ISM case. The top panel shows the flow speed normalized to u_0 for the $\alpha_H = 0.0$ and $\alpha_H = 0.5$ models. The middle panel shows various constituents of pressure for the $\alpha_H = 0.0$ run: the thermal pressure P_{th} , the pressures of ‘adolescent’ particles that crossed the shock 1, 2, 3 and 4 times (P_1 , P_2 , P_3 and P_4 , respectively), the pressure of particles that have crossed 5 and more times $P_{>5}$ and the magnetic turbulence pressure P_w , all of the above are normalized to the far upstream momentum flux Φ_{P0} . The bottom panel shows the same quantities for $\alpha_H = 0.5$.

Figure 3 shows an overlap in the curves for the flow speed $u(x)$ in the $\alpha_H = 0$ and $\alpha_H = 0.5$ models, and only close to the subshock $u(x)$ falls off more rapidly towards the subshock in the $\alpha_H = 0.5$ case, resulting eventually in a lower r_{sub} . This means that for the high energy particles, which diffuse far upstream, the acceleration process will go on in about the same way with and without moderate turbulence dissipation (and the acceleration efficiency will be preserved with changing α_H). For lower energy particles, however, there will be observable differences in the energy spectrum. The $\alpha_H = 1.0$ case has a significantly smoother precursor, which is not unusual, given the lower maximal energy of the accelerated particles in this case (because of the magnetic field remaining low). The thermal gas temperatures $T(x)$ plotted in the bottom panels of Figure 3 were calculated from the thermal pressure $P_{\text{th}}(x)$ using (14) and show that the temperature becomes high well in front of the subshock.

In Figure 4 the subshock region for the hot ISM case is shown enlarged, and we can compare details of the models with ($\alpha_H = 0.5$) and without dissipation ($\alpha_H = 0.0$). In the absence of turbulence dissipation, the thermal pressure P_{th} remains low upstream (see the middle panel), and the subshock transition is dominated by the magnetic pressure P_w . For $\alpha_H = 0.5$ (the bottom panel) the thermal pressure P_{th} just before the shock increases enough to become comparable with the magnetic pressure, but also the heating-boosted particle injection brings up the pressures of the ‘adolescent’ particles. As the plot shows, for $\alpha_H = 0.5$ the pressures produced by the first and second time returning particles (P_1 and P_2) are not small compared to P_{th} and P_w just upstream of the shock, which contributes to the reduction of r_{sub} described above. However, the pressure of the ‘mature’ particles, $P_{>5}$, doesn’t change much, which is a result of the non-linear response of the shock structure to the increased injection.

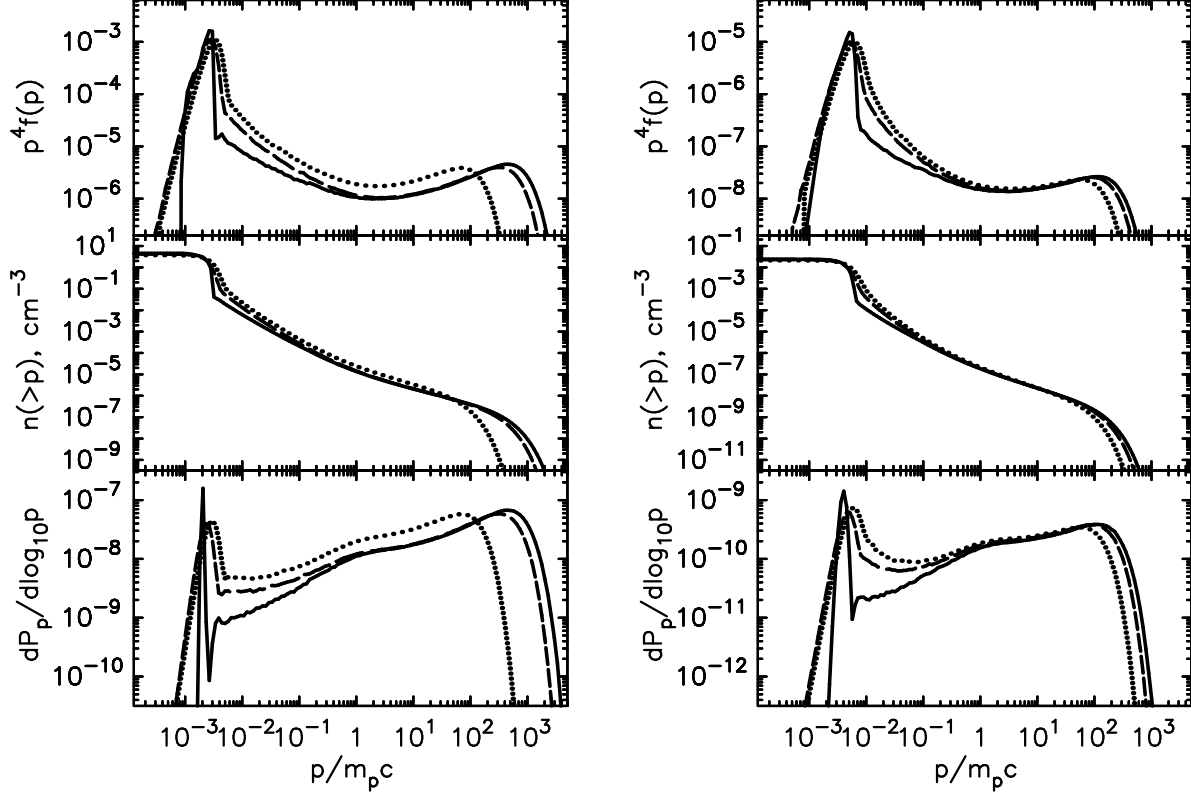


Fig. 5.— Results of non-linear simulations in the cold ISM(left) and hot ISM (right) with different values of α_H . Line styles as in Fig. 3. The plotted quantities are: the particle distribution function in the shock frame $f(p)$ multiplied by p^4 (the normalization is such that $\int 4\pi p'^2 f(p') dp' = n$, n being the number density in cm^{-3} , and $p' = p/(m_p c)$), the number of particles $n(>p)$ with momentum greater than p (in cm^{-3}) and the particle pressure (in dynes per cm^2) per decade of normalized momentum $dP_p/d\log_{10} p/(m_p c)$. All quantities are calculated downstream at $x = +6r_{g0}$.

The low energy parts of the particle distribution functions shown in Figure 5 are significantly different for models with and without dissipation in both the cold ISM and the hot ISM cases. The apparent widening of the thermal peak reflects the increase in the downstream gas temperature T_2 . The differences extend from the thermal peak to mildly superthermal momenta $0.2 m_p c$, which shows an increased population of the ‘adolescent’ particles with speeds up to $v \approx 0.2c \approx 12u_0$ when the turbulence dissipation operates. The high energy ($p > 0.2 m_p c$) parts of the spectra for $\alpha_H = 0$ and $\alpha_H = 0.5$ are similar (except for a lower p_{\max} due to a lower value of the amplified field in the $\alpha_H = 0.5$ case), confirming our assertion about the preservation of the particle acceleration efficiency. The increased population of the low-energy particles just above the thermal peak should influence the shock’s X-ray emission.

The characteristic concave curvature of the particle spectra above the thermal peak is clearly seen in the top panels of Figure 5. These shocks are strongly nonlinear and, as the bottom panels in Figure 5 show, most of the pressure is in the highest energy particles. For these examples, 60 to 80 percent of the downstream momentum flux is in CR particles. The number of particles producing this pressure is small, however, and as the plots in the middle panels show, the fraction of particles above the thermal peak is on the order of 10^{-3} , and the fraction of particles above 1 GeV is around 10^{-6} in all cases. In addition to the pressure (and energy) in the distributions shown, a sizable fraction of shock ram kinetic energy flux escapes at the FEB.

To summarize, for both the unmodified (Fig. 1) and modified (Fig. 2) cases, M_{s1} drops and f_{cr} grows as α_H increases. The surprising result is that $B_{\text{eff}2}$ can increase in the unmodified shock as α_H goes up if r_{tot} is large enough. This indicates that the boosted injection efficiency (i.e., larger f_{cr}) outweighs the effects of field damping. This doesn’t happen in the modified case (top panel of Fig. 2) because of the nonlinear effects from the increased injection. From Fig. 4 we see that the boosted injection results in a smoother subshock and this makes it harder for low energy adolescent particles to gain energy. Once particles reach a high enough momentum ($p \gtrsim 0.2m_p c$; see the top panel of Fig. 5) they are able to diffuse far enough upstream where the boost in injection has a lesser effect.

We must emphasise again that these results are very sensitive to the physics of particle injection at the subshock. It is difficult to predict how the nonlinear results would change if a different model of injection was used, but we can refer the reader to the work of Amato & Blasi (2006), who performed a similar calculation using the threshold injection model with a different diffusion coefficient.

The free escape boundary in our simulation was relatively close to the shock ($x_{\text{FEB}} = -10^5 r_{g0} \approx -3 \times 10^{-4}$ pc), and the maximum accelerated particle energy was on the order

of hundreds of GeV. These quantities, chosen to save computation time, are several orders of magnitude short of typical SNR values. Nevertheless, we don't believe our results will be changed qualitatively if p_{\max} is increased. The reason is that even with our relatively low p_{\max} , the fraction of internal energy in relativistic particles is still large and the volume-averaged value of the polytropic index of the precursor plasma, $\langle\gamma(x < 0)\rangle$, as shown in Tables 1 and 2, is much closer to the 4/3 of a fully relativistic gas than to 5/3 for a non-relativistic one. Increasing p_{\max} will not lower the polytropic index of the gas any further and, consequently, the plasma compression and the subsequent acceleration efficiency will not change significantly (see Berezhko & Ellison 1999).

4. Conclusions

We have parameterized magnetic turbulence dissipation as a fraction of turbulence energy generation and included this effect in our Monte Carlo model of strongly nonlinear shocks undergoing efficient DSA. The energy removed from the turbulence goes directly into the thermal particle population in the shock precursor. The Monte Carlo simulation self-consistently reacts to the changes in precursor heating and adjusts the injection of thermal particles into the DSA mechanism, as well as other nonlinear effects of DSA, accordingly.

Our two most important results are, first, that even a small rate ($\sim 10\%$) of turbulence dissipation can drastically increase the precursor temperature, and second, that the precursor heating boosts particle injection into DSA by a large factor. The increase in particle injection modifies the low-energy part of the particle spectrum but, due to nonlinear feedback effects, does not significantly change the overall efficiency or the high energy part of the spectrum. Both the precursor heating and modified spectral shape that occur with dissipation may have observable consequences.

The fact that the shock back-reaction to the increased injection prevents the acceleration efficiency from changing significantly is a clear consequence of the non-linear structure of the system. The boosted particle injection additionally smoothes the flow speed close to the subshock, which makes it harder for particles returning upstream to gain energy. As a result, the population of the high energy particles is not much changed and, because those particles carry the bulk of the CR pressure P_{cr} which drives the streaming instability, the amplification of the magnetic field is not strongly affected by the heating-boosted particle injection.

The parameterization we use here is a simple one and a more advanced description of the turbulence damping may change our results. In our model the energy drained from

the magnetic turbulence, at all wavelengths, is directly ‘pumped’ into the thermal particles. Superthermal particles only gain extra energy due to heating because the thermal particles were more likely to return upstream and get accelerated. In a more advanced model of dissipation, where energy cascades from large-scale turbulence harmonics to the short-scale ones, the low energy CRs might gain energy directly from the dissipation. It is conceivable that cascading effects might increase the overall acceleration efficiency, the magnetic field amplification, and increase the maximum particle energy a shock can produce.

It is also possible that non-resonant turbulence instabilities play an important role in magnetic field amplification (e.g., Pelletier et al. 2006). This opens another possibility for the turbulence dissipation to produce an increase in the magnetic field amplification. For instance, Bykov & Toptygin (2005) proposed a mechanism for generating long-wavelength perturbations of magnetic fields by low energy particles. If such a mechanism is responsible for generation of a significant fraction of the turbulence that confines the highest energy particles, then the increased particle injection due to the precursor heating may raise the maximum particle energy and, possibly, the value of the amplified magnetic field.

While our model is for the most part phenomenological as far as particle transport, injection and acceleration, magnetic field generation, and dissipation are concerned, it allows us to investigate the coupled nonlinear effects in a shock undergoing efficient DSA and MFA. The more efficient DSA is, the more basic considerations of momentum and energy conservation determine the shock structure and our model describes these effects fully.

We thank the anonymous referee for a number of very valuable comments and suggestions. D. C. E. and A. V. wish to acknowledge support from NASA grants NNH04Zss001N-LTSA and 06-ATP06-21. A. M. B. acknowledges support from RBRF grant 06-02-16884.

A. Comments on PIC simulations of MFA

There are two basic reasons why the problem of MFA in nonlinear diffusive shock acceleration (NL-DSA) is particularly difficult for particle-in-cell (PIC) simulations. The first is that PIC simulations must be done fully in three dimensions to properly account for cross-field diffusion. As Jones et al. (1998) proved from first principles, PIC simulations with one or more ignorable dimensions unphysically prevent particles from crossing magnetic field lines. In all but strictly parallel shock geometry,¹⁰ a condition which never occurs in strong

¹⁰Parallel geometry is where the upstream magnetic field is parallel to the shock normal.

turbulence, cross-field scattering is expected to contribute importantly to particle injection and must be fully accounted for if injection from the thermal background is to be modeled accurately.

The second reason is that, in nonrelativistic shocks, NL-DSA spans large spatial, temporal, and momentum scales. The range of scales is more important than might be expected because DSA is intrinsically efficient and nonlinear effects tend to place a large fraction of the particle pressure in the highest energy particles (see Fig. 5). The highest energy particles, with the largest diffusion lengths and longest acceleration times, feedback on the injection of the lowest energy particles with the shortest scales. The accelerated particles exchange their momentum and energy with the incoming thermal plasma through the magnetic fluctuations coupled to the flow. This results in the flow being decelerated and the plasma being heated. The structure of the shock, including the subshock where fresh particles are injected, depends critically on the highest energy particles in the system.

A plasma simulation must resolve the electron skin depth, c/ω_{pe} , i.e., $L_{\text{cell}} < c/\omega_{pe}$, where $\omega_{pe} = [4\pi n_e e^2/m_e]^{1/2}$ is the electron plasma frequency and L_{cell} is the simulation cell size. Here, n_e is the electron number density, m_e is the electron mass and c and e have their usual meanings. The simulation must also have a time step small compared to ω_{pe}^{-1} , i.e., $t_{\text{step}} < \omega_{pe}^{-1}$.

If we wish to follow the acceleration of protons in DSA to the TeV energies present in SNRs we must have a simulation box that is as large as the upstream diffusion length of TeV protons, i.e., $\kappa(\text{TeV})/u_0 \sim r_g(\text{TeV})c/(3u_0)$, where κ is the diffusion coefficient, $r_g(\text{TeV})$ is the gyroradius of a TeV proton, u_0 is the shock speed, and we have assumed Bohm diffusion. The simulation must also be able to run for as long as the acceleration time, τ_{acc} , of TeV protons, where $\tau_{\text{acc}} \sim Ec/(eBu_0^2)$. Here, E is the relativistic energy and B is some average magnetic field. The spatial condition gives

$$\frac{\kappa(E_{\text{max}})/u_0}{(c/\omega_{pe})} \sim 6 \times 10^{11} \left(\frac{B}{\mu\text{G}}\right)^{-1} \left(\frac{n_e}{\text{cm}^{-3}}\right)^{1/2} \left(\frac{E_{\text{max}}}{\text{TeV}}\right) \left(\frac{f}{1836}\right)^{1/2} \left(\frac{u_0}{1000 \text{ km s}^{-1}}\right)^{-1}, \quad (\text{A1})$$

for the number of cells *in one dimension*. The factor $f = m_p/m_e$ is the proton to electron mass ratio. From the acceleration time condition, the required number of time steps is,

$$\frac{\tau_{\text{acc}}(E_{\text{max}})}{\omega_{pe}^{-1}} \sim 6 \times 10^{14} \left(\frac{u_0}{1000 \text{ km s}^{-1}}\right)^{-2} \left(\frac{B}{\mu\text{G}}\right)^{-1} \left(\frac{n_e}{\text{cm}^{-3}}\right)^{1/2} \left(\frac{E_{\text{max}}}{\text{TeV}}\right) \left(\frac{f}{1836}\right)^{1/2}. \quad (\text{A2})$$

Even with $f = 1$ these numbers are obviously far beyond any conceivable computing capabilities and they show that approximate methods are essential for studying NL-DSA.

One approximation that is often used is a hybrid PIC simulation where the electrons are treated as a background fluid. To get the most optimistic estimate of the requirements

in this case we can take the minimum cell size as the thermal proton gyroradius, $r_{g0} = \sqrt{2m_p E_{th}}/(eB)$, and set the maximum box size to the gyroradius at 1 TeV (instead of the diffusion length). Now, the number of cells, *again in one dimension*, is:

$$\frac{r_g(E_{\max})}{r_{g0}} = 1 \times 10^6 \left(\frac{E_{th}}{\text{keV}} \right)^{-1/2} \left(\frac{E_{\max}}{\text{TeV}} \right). \quad (\text{A3})$$

The number of time steps can be taken as $\tau_{\text{acc}}/\tau_{\text{gp}}$, where τ_{gp} is the thermal proton gyroperiod. This gives the number of time steps to reach 1 TeV,

$$\frac{\tau_{\text{acc}}(E_{\max})}{\tau_{\text{gp}}} = 1.5 \times 10^7 \left(\frac{u_0}{1000 \text{ km s}^{-1}} \right)^{-2} \left(\frac{E_{\max}}{\text{TeV}} \right). \quad (\text{A4})$$

These combined spatial and temporal requirements, even for the most optimistic case of a hybrid simulation with an unrealistically large t_{step} , are well beyond existing computing capabilities unless exceptionally clever shortcuts, such as adaptive mesh refinement, are devised or a maximum energy well below 1 TeV is used.

Since the three-dimensional requirement is fundamental and relaxing it eliminates cross-field diffusion, restricting the energy range is the best way to make the problem assessable to hybrid PIC simulations. However, since producing relativistic particles from nonrelativistic ones is an essential part of the NL problem, the energy range must comfortably span $m_p c^2$ to be realistic. If $E_{\max} = 10 \text{ GeV}$ is used, with $u_0 = 5000 \text{ km s}^{-1}$, and $E_{th} = 10 \text{ MeV}$, equation (A3) gives ~ 100 and equation (A4) gives $\sim 10^4$. Now, the computation may be possible, even with the 3-D requirement, but the hybrid simulation can't fully investigate MFA since electron return currents are not modeled. The exact microscopic description of the system is not currently feasible.

It's hard to make a comparison in run-time between PIC simulations and the Monte Carlo technique used here since we are not aware of any published results of 3-D PIC simulations of nonrelativistic shocks that follow particles from fully nonrelativistic to fully relativistic energies. A direct comparison of 1-D hybrid and Monte Carlo codes was given in Ellison et al. (1993) for energies consistent with the acceleration of diffuse ions at the quasi-parallel Earth bow shock. Three-dimensional hybrid PIC results for nonrelativistic shocks were presented in Giacalone & Ellison (2000) and these were barely able to show injection and acceleration given the computational limits at that time. As for the Monte Carlo technique, all of the 16 nonlinear simulations presented in this paper were completed in approximately 4 days on a parallel computing cluster, employing around 30 processors; enough statistical information was accumulated to restrict the uncertainty in the self-consistent value of r_{tot} to 5 percent. Increasing the dynamic range of the simulations to SNR-like energies ($E_{\max} \approx 1 \text{ PeV}$) would require 2-4 times more computation time. The performance of the

Monte Carlo code is mostly limited by the productivity of its algorithm rather than by physical constraints, and can probably be significantly improved.

Despite these limitations, PIC simulations are the only way of self-consistently determining the plasma physics of collisionless shocks. All things considered, the most difficult aspect of the MFA problem in NL-DSA, and the one least assessable to analytic and Monte Carlo techniques, remains the initial injection of thermal particles in the large amplitude waves and time varying structure of the subshock. PIC simulations are the only way to obtain essential information in this critical regime (e.g., Niemiec et al. 2008; Spitkovsky 2008).

B. Analytic Precursor Approximation procedure

Here we describe our Analytic Precursor Approximation (APA) where we introduce thermal particles into the MC simulation, not far upstream, but at some position $x_{\text{APA}} < 0$ close to the subshock. This procedure has two purposes. First, it saves computational time because we don't have to trace these particles along the extended shock precursor. Second, we use the APA to simulate the turbulence dissipation in the shock precursor: with this procedure we incorporate the analytic description of the heating of the thermal gas due to the turbulence dissipation into the Monte Carlo model of particle transport.

In the next two subsections we describe how the momentum and energy fluxes in shock precursor are calculated in the absence of turbulence dissipation (part B.1), and then explain how this scheme is changed when the Analytic Precursor Approximation procedure is invoked to model the thermal plasma heating by turbulence dissipation (part B.2).

B.1. Precursor without Analytic Approximation

B.1.1. Inherent Quasi-Adiabatic Heating and Subshock Definition in Monte Carlo Simulation

It is worth pointing out that even if the turbulence dissipation is not included in our simulation, particles in the precursor will still be weakly heated. Just like an ideal collisionless gas put in a slowly shrinking volume will heat up adiabatically due to elastic collisions of particles with in-moving walls, the particles in our MC simulation traveling in a compressing shock precursor will heat up according to the adiabatic law $P_{\text{th}} \propto \rho^\gamma \propto u^{-\gamma}$ due to elastic scattering in the decelerating local plasma frame. This will be true as long as the particles have enough time to adjust to the changing flow speed. Quantitatively, the criterion for

adiabatic heating is

$$\tau_{\text{coll}} \ll \tau_{\text{comp}}, \quad (\text{B1})$$

where the collision time, τ_{coll} , is the ratio of the mean free path to the particle speed, (for nonrelativistic particles $\tau_{\text{coll}} = m_p c / (e B_{\text{eff}})$), and the compression time τ_{comp} is the temporal scale on which the speed of plasma that the particle is traveling in changes significantly, that is, by a value comparable to the particle speed v . Assuming $v \ll u$, τ_{comp} is approximately the ratio of the length on which the flow speed changes by v to the advection speed u : $\tau_{\text{comp}} = (v / |(du/dx)|) / u$. It also follows from the definition of τ_{coll} that the angular distribution of the particles remains isotropic if (B1) is true. The condition (B1) is therefore

$$\left| \frac{du}{dx} \right| \ll \frac{v e B_{\text{eff}}}{u m_p c}, \quad (\text{B2})$$

restricting the flow speed gradient to small enough values, where adiabatic compression operates.

If the magnitude of the flow speed gradient $|du/dx|$ is too large and (B1) doesn't hold, the increase of particle energies will be faster than adiabatic, and the angular distribution function will become non-isotropic, with more particles moving against the gradient than along it in the plasma frame. One obvious place where this occurs is the subshock. In our simulation, the subshock in the non-linear, self consistent solution gains a finite width, but the flow speed jump at the subshock remains strong and rapid enough to efficiently accelerate particles. We define the point at which the transition from the adiabatic to the non-adiabatic regime occurs, x_{tr} , by the following condition:

$$\tau_{\text{coll}}(x_{\text{tr}}) = \frac{1}{3} \tau_{\text{comp}}(x_{\text{tr}}), \quad (\text{B3})$$

or, in terms of quantities available in the simulation,

$$\left. \frac{du}{dx} \right|_{x_{\text{tr}}} = - \frac{1}{3} \frac{v e B_{\text{eff}}(x_{\text{tr}})}{u(x_{\text{tr}}) m_p c}, \quad (\text{B4})$$

where $v = \sqrt{2k_B T(x_{\text{tr}})/m_p}$, in which case $|x_{\text{tr}}|$ is comparable to the local convective mean free path of a thermal particle. The factor $1/3$ is chosen arbitrarily but our results are insensitive to it. Close to the shock, at $x_{\text{tr}} < x < 0$, the flow speed drops so rapidly that the particles are heated in a non-adiabatic fashion. We can think of the non-adiabatic region as a subshock with a finite thickness $|x_{\text{tr}}|$, and it is then reasonable to define the pre-subshock quantities (denoted with index '1') as the values at $x = x_{\text{tr}}$: $u_1 = u(x_{\text{tr}})$, $r_{\text{sub}} = u(x_{\text{tr}})/u(x > 0)$, etc. We note that Equation B4 is only used to define the position of the subshock and is not used in any calculations.

B.1.2. Direct Calculation of Momentum and Energy Fluxes

The flux of momentum $\Phi_P(x)$ defined in (18) is used in our simulation to calculate the smoothing of the precursor plasma flow $u(x)$, and the flux of energy $\Phi_E(x)$ defined in (23) is used to calculate the compression ratio r_{tot} consistent with the particle acceleration. The moments of the particle distribution function in (18) and (23) are the components of the stress tensor. If the plasma heating by turbulence dissipation is not modeled, and the Analytic Precursor Approximation procedure is not performed, then these moments are calculated in our simulation as described below. At select positions on the numerical grid spanning from far upstream to some position downstream from the subshock we sum the contributions of the particles that cross these positions to calculate the following:

$$\int p_x v_x f(x, \mathbf{p}) d^3p = \sum_i p_{i,x} v_{i,x} w_i, \quad (\text{B5})$$

$$\int K v_x f(x, \mathbf{p}) d^3p = \sum_i K_i v_{i,x} w_i. \quad (\text{B6})$$

Here the summation is taken over all particles crossing the position x at which the moments are calculated. The index i represents the considered particle, p_x (v_x) is the x -component of a particle's momentum (velocity), K is the kinetic energy, all measured in the shock frame, and w is the weight of the particle defined as

$$w_i = \left| \frac{u_0}{v_{i,x}} \right| \frac{n_0}{N_p}. \quad (\text{B7})$$

In this definition the ratio $|u_0/v_{i,x}|$ is the weighting factor accounting for the fact that in our simulation particles crossing the position x at some angle to the flow do it less frequently than particles crossing parallel to the flow, n_0 is the upstream number density of the plasma and N_p is the number of simulation particles.

If the particle distribution is isotropic in the local plasma frame moving at speed $u(x)$ relative to the shock, then the quantities calculated in (B5) and (B6) can be expressed in the following way:

$$\int p_x v_x f(x, \mathbf{p}) d^3p = \rho(x) u^2(x) + P_p(x), \quad (\text{B8})$$

$$\int K v_x f(x, \mathbf{p}) d^3p = \frac{1}{2} \rho(x) u^3(x) + w_p(x) u(x), \quad (\text{B9})$$

where $P_p(x)$ is the pressure and $w_p(x)$ is the enthalpy of the particles. In the vicinity of the subshock, however, the isotropy assumption breaks down (see the discussion in Appendix B.1.1 and the note on anisotropy in Appendix C), and the concept of isotropic

pressure is not applicable. The fact that we directly calculate the moment of the distribution function in (18) by evaluating the sum (B5), instead of approximating the momentum flux with (B8), ensures that we properly account for the effects of the anisotropy of particle distribution. This turns out to be important for self-consistently determining the flow speed $u(x)$ near the subshock, which controls the subshock compression and the subsequent particle injection and acceleration efficiency.

When plasma heating by turbulence dissipation is modeled, we replace the calculation (18) with an analytic approximation assuming isotropic particle pressure, but we take special care to be certain that this approximation is only done far enough from the shock, where the isotropy approximation is applicable. This procedure is described below.

B.2. Modeling Precursor Heating with the APA

B.2.1. Particle Introduction Position

The position at which the thermal particles are introduced must be close enough to the shock so that the analytic description of heating applies to most of the precursor extent, but far enough away from the non-adiabatic region $x_{\text{tr}} < x < 0$, so that the analytic approximation remains valid where applied. In our simulation we chose the particle introduction position, x_{APA} , so that the condition (B1) is only marginally valid at this position. We formalize it as

$$\tau_{\text{coll}}(x_{\text{APA}}) = M\tau_{\text{comp}}(x_{\text{APA}}), \quad (\text{B10})$$

which is equivalent to

$$\left. \frac{du}{dx} \right|_{x_{\text{APA}}} = -M \frac{veB_{\text{eff}}(x_{\text{APA}})}{u(x_{\text{APA}})m_p c}. \quad (\text{B11})$$

where we chose $M = 0.1$ and $v = \sqrt{2k_B T_0/m_p}$. At $x < x_{\text{APA}}$ we describe the thermal particle distribution function as a Maxwellian with the temperature defined by (13) and (14), and at $x > x_{\text{APA}}$ we use the Monte Carlo simulation to describe the more complex particle dynamics.

B.2.2. Momentum Space Distribution of Introduced Particles

In order to include the effects of heating in the model, we must introduce thermal particles at x_{APA} as if they were heated in the precursor, i.e., their temperature $T(x_{\text{APA}})$ must be determined by (13) and (14). We therefore choose the magnitude of every particle's momen-

tum p in the local plasma frame distributed according to Maxwell-Boltzmann distribution with probability density

$$f(p) = \frac{4}{\sqrt{\pi}} \left(\frac{1}{2mk_B T(x_{\text{APA}})} \right)^{3/2} p^2 \exp \left(-\frac{p^2}{2mk_B T(x_{\text{APA}})} \right). \quad (\text{B12})$$

The angular distribution of momenta of the introduced particles is a major issue of concern in doing simulation like ours because it determines the particle injection rate. We are replacing the dynamics of particles at $x < x_{\text{APA}}$ with an analytical description, consequently we must distribute particles in p -space at x_{APA} the way they would be distributed having traveled from far upstream and reaching x_{APA} *for the first time*. This is equivalent to calculating a p -space distribution of particles incident on a *fully absorbing boundary* at x_{APA} after scattering in a non-uniform flow $u(x)$. This is easy to do analytically if all particles have a plasma frame speed v less than the flow speed $u(x_{\text{APA}})$ (because then all particles crossing position x_{APA} do it for the first and the last time), and fairly complicated otherwise. We assume $v < u(x_{\text{APA}})$ in further reasoning, which is justified by the fact that we find $M_s(x_{\text{APA}}) \gtrsim 3$ in most cases.

As was stated earlier, we assume that the angular distribution of momenta of the introduced thermal particles is isotropic in the plasma frame. When these particles cross a position fixed in the shock frame, their flux must be ‘weighted’ to account for the fact that the number of particles arriving at x_{APA} in a unit time is proportional to the cosine of the angle that their shock frame velocity \mathbf{v}_{sf} makes with the x -axis. This can be done by assuming a probability density of $\mu = v_x/v$ (v is the magnitude of the particle plasma frame velocity and v_x its x -component) as

$$f(\mu) = \frac{1}{2} \left(1 + \mu \frac{v}{u} \right), \quad (\text{B13})$$

where $u = u(x_{\text{APA}})$. It is normalized so that the probability $Pr(\mu_0 < \mu < \mu_0 + d\mu_0) = f(\mu_0)d\mu_0$, and the functional form of (B13) comes from the assumption that $f(\mu) \propto v_{\text{sf}, x} = u + \mu v$.

B.2.3. Heating of the Upstream Plasma

After the thermal particles are introduced at x_{APA} and start to propagate in the shocked flow, we have to calculate the momentum and energy fluxes throughout the shock, for use in our iterative procedure. Because we didn’t propagate the thermal particles at $x < x_{\text{APA}}$, and because we must model the momentum flux redistribution between the turbulence and

the thermal particles due to heating, we calculate the corresponding moments of particle distribution function the following way:

$$\int p_x v_x f(x, \mathbf{p}) d^3 p = \begin{cases} \sum_{all\ i} p_{i,x} v_{i,x} w_i, & \text{if } x > x_{APA}, \\ \rho(x) u^2(x) + P_{th}(x) + \sum_{i \in CR} p_{i,x} v_{i,x} w_i, & \text{if } x < x_{APA}, \end{cases} \quad (B14)$$

$$\int K v_x f(x, \mathbf{p}) d^3 p = \begin{cases} \sum_{all\ i} K_i v_{i,x} w_i, & \text{if } x > x_{APA}, \\ \frac{1}{2} \rho(x) u^3(x) + \frac{\gamma}{\gamma - 1} P_{th}(x) u(x) + \sum_{i \in CR} K_i v_{i,x} w_i, & \text{if } x < x_{APA}. \end{cases} \quad (B15)$$

The summation for $x > x_{APA}$ is taken over all the particles crossing position x , and for $x < x_{APA}$ the summation index $i \in CR$ only includes the CR (i.e., injected) particles, while the contribution of the thermal particles is replaced by the analytic approximation of this contribution. The thermal pressure in this approximation is taken from the solution of (13). For $\alpha_H = 0$ the equations (B14) and (B15) produce the same results (within intrinsic random deviations of the Monte Carlo code) as the calculation (B5) and (B6).

In the region $x_{APA} < x < 0$ the heating due to L is ignored. This may, in principle, underestimate the heating of the upstream gas, but we find that this is a negligible effect. We prove it by running a simulation with another x_{APA} , even farther away from the subshock, and making sure that the results are not affected significantly.

C. Note on Differentiation between Thermal and CR particles

As was mentioned earlier, we call a particle a thermal particle or a CR one based on its history: a CR particle is one that has gotten injected into the acceleration process by having crossed the shock from the downstream to the upstream region at least once¹¹. This criterion is used at two places in the model. First, it is used to calculate the spectrum of pressure driving the CR streaming instability $P_{cr}(x, p)$: only the contribution of injected particles is included in $P_{cr}(x, p)$. Second, when we calculate the thermal particle pressure $P_{th}(x)$ at $x < x_{APA}$ using (9) and (13), and then introduce thermally distributed particles at $x = x_{APA}$ and continue the calculation of pressure for $x > x_{APA}$ from their trajectories as they elastically scatter in the flow, we implicitly assume that the dissipated energy of the

¹¹Although the shock gains a finite width in the Monte Carlo simulation, we define the backward shock crossing as moving from $x > 0$ to $x < 0$.

turbulence goes directly into the thermal energy of the particles that have not been injected, i.e., thermal particles in our definition.

If a description of particle-wave interactions in strong turbulence existed that explicitly described how particles of different energies participated differently in the instability generation and the turbulence dissipation, a criterion like ours would not be needed. However, such a description is not available and we believe that our way of separating thermal and superthermal (CR) particles for purposes of describing the instability growth and the turbulence dissipation grasps the essential non-linear effects in the shock structure. PIC simulations are, in principle, able to tackle this problem exactly but, as we mentioned earlier, they are extremely computationally expensive.

We would like to point out an important consequence of our using the ‘thermal leakage’ model of particle injection into the acceleration process. Our simulation follows histories of charged particles from their ‘childhood’, when their speeds in the plasma frame are small compared to the bulk flow speed, to ‘maturity’, when they become relativistic. Unlike most semi-analytic descriptions of DSA, our model doesn’t skip the ‘adolescence’ stage of particles, when after one or a few shock crossings the particles have speeds comparable to or slightly greater than the bulk flow speed. In the absence of these ‘adolescent’ particles, it is typically assumed that the jump in only the thermal particle pressure across the subshock determines the strength of the latter, and the superthermal part of the particle spectrum is continuous at the subshock and does not influence it. But the ‘adolescent’ particles that the Monte Carlo model does describe are not energetic enough to be insensitive to the subshock, and at the same time they have a strong anisotropy in the plasma frame, and therefore do not obey the Rankine-Hugoniot relations. This modifies the conservation laws across the subshock, because in the total kinetic pressure $P_p(x) = P_{\text{th}}(x) + P_{\text{cr}}(x)$ the term $P_{\text{cr}}(x)$ is not continuous at the subshock due to the contribution of the intermediate energy particles that it contains.

D. Compression ratio, Turbulence and Escaping Particles

Equation (10) in Ellison et al. (1990b) relates the fraction of energy flux carried away by escaping particles q_{esc} to the total shock compression ratio, r_{tot} . It assumes no magnetic field amplification and a polytropic index of downstream gas equal to 5/3 (in other words, neglects the effect of relativistic particles on the overall compressibility of the gas). In order to search for a r_{tot} consistent with the shock structure and with particle escape, we derive a similar relationship that would account for the presence of magnetic turbulence and for the contribution of the relativistic particles. The problem is complicated by having particles of intermediate (mildly relativistic) energies and by the value of the magnetic field dependent

on the particle acceleration.

Writing equations (15), (16) and (21) for a point downstream of the shock, sufficiently far from it, so that the distribution of particle momenta is isotropic, and the approximations (B8) and (B9) are valid, and denoting the corresponding quantities by index ‘2’, we get:

$$\rho_2 u_2 = \rho_0 u_0, \quad (\text{D1})$$

$$\rho_2 u_2^2 + P_{p2} + P_{w2} = \rho_0 u_0^2 + P_{p0} + P_{w0} \equiv \Phi_{p0}, \quad (\text{D2})$$

$$\frac{1}{2} \rho_2 u_2^3 + w_{p2} u_2 + F_{w2} + Q_{\text{esc}} = \frac{1}{2} \rho_0 u_0^3 + w_{p0} u_0 + F_{w0} \equiv \Phi_{E0}. \quad (\text{D3})$$

The particle gas enthalpy w_p is $w_p = \epsilon_p + P_p$, and the internal energy ϵ_p of gas is proportional to the pressure P_p . Introducing the quantity $\bar{\gamma}$ so that $\epsilon_p = P_p/(\bar{\gamma} - 1)$, one can write

$$w_p u = \frac{\bar{\gamma}}{\bar{\gamma} - 1} P_p u \quad (\text{D4})$$

The value of $\bar{\gamma}$ is averaged over the whole particle spectrum, and it ranges between 5/3 for a nonrelativistic and 4/3 for an ultra-relativistic gas. The local value of $\bar{\gamma}$ can be easily calculated in our code from the particle distribution, along with P_p and ϵ_p , as $\bar{\gamma} = 1 + P_p/\epsilon_p$. Similarly, one can define $\bar{\delta} = F_w/(u P_w)$ and calculate a local value of $\bar{\delta}$ anywhere in the code in order to express

$$F_w = \bar{\delta} \cdot P_w u. \quad (\text{D5})$$

For $V_G \ll u$ and Alfvénic turbulence, one expects $\bar{\delta} \approx 3$, [see eq. (12)].

Substituting (D4) and (D5) into the above equations and introducing $r_{\text{tot}} = u_0/u_2$, we can eliminate ρ_2 using (D1) and P_{p2} using (D2), which allows us to express from (D3) the quantity $q_{\text{esc}} \equiv Q_{\text{esc}}/\Phi_{E0}$ as

$$q_{\text{esc}} = 1 + \frac{A/r_{\text{tot}}^2 - B/r_{\text{tot}}}{C}, \quad (\text{D6})$$

where

$$A = \frac{\bar{\gamma}_2 + 1}{\bar{\gamma}_2 - 1}, \quad (\text{D7})$$

$$B = \frac{2\bar{\gamma}_2}{\bar{\gamma}_2 - 1} \left(1 + \frac{P_{p0} + P_{w0} - P_{w2}}{\rho_0 u_0^2} \right) + \frac{2\bar{\delta}_2 P_{w2}}{\rho_0 u_0^2}, \quad (\text{D8})$$

$$C = 1 + \frac{2\bar{\gamma}_0}{\bar{\gamma}_0 - 1} \frac{P_{p0}}{\rho_0 u_0^2} + \frac{2\bar{\delta}_0 P_{w0}}{\rho_0 u_0^2}. \quad (\text{D9})$$

Note that $\rho_0 u_0^2/P_{p0} = \bar{\gamma}_0 M_s^2$, where $\bar{\gamma}_0 = \gamma = 5/3$ due to the absence of CRs far upstream, and, because we assume a seed turbulence far upstream, that provides a Bohm regime of scattering to all particles, one can write that far upstream $\Delta B \approx B_0$, making $\rho_0 u_0^2/P_{w0} = 2M_A^2$.

The quantity q_{esc} is readily available in the simulation after the end of any iteration. Comparing it to the value predicted by (D6), we evaluate the self-consistency of the solution and make the correction to r_{tot} , if necessary, for further iterations. For making these corrections it is helpful to use in the simulation the inverse of (D6), the physically relevant branch of which is

$$r_{\text{tot}} = \frac{2A}{B - \sqrt{B^2 - 4AC(1 - q_{\text{esc}})}}. \quad (\text{D10})$$

It is important to emphasise here that an iterative procedure similar to (19) is still required to find the compression ratio r_{tot} of a non-linearly modified shock, because quantities q_{esc} , P_{w2} and $\bar{\gamma}_2$ depend on r_{tot} , so (D10) only provides a practical way to perform the iterations.

E. Note on Subshock Properties in the Presence of MFA

Kang et al. (2002) showed, using a thermal leakage injection model similar to what is used here, that in a non-linearly modified shock with Bohm diffusion and a sonic Mach number M_{s0} , the subshock sonic Mach number scales as $M_{s1} \sim 2.9M_{s0}^{0.13}$ with the corresponding subshock compression ratio $r_{\text{sub}} = 4/(1 + 3/M_{s1}^2)$. Numerically, for $M_{s0} = 400$ it gives $M_{s1} \approx 6.3$ and $r_{\text{sub}} \approx 3.7$.

The model of Kang et al. (2002) does not include magnetic field amplification and, as we have shown, in our case the values of the subshock sonic Mach number and compression ratio are quite different. For instance, for our model with MFA, but without magnetic turbulence damping ($\alpha_H = 0$) we have found that $M_{s0} = 426$ results in $M_{s1} \approx 44$ and $r_{\text{sub}} \approx 3$. The value of M_{s1} in the absence of precursor plasma heating is determined by the high CR pressure $P_{\text{cr}}(x)$, and the value of r_{sub} in the high Mach number shock with MFA is largely controlled by the pressure of the amplified magnetic turbulence $P_w(x)$ rather than by the thermal pressure $P_{\text{th}}(x)$. The situation is changed when the turbulence dissipation operates, because it dampens $P_w(x)$ and increases $P_{\text{th}}(x)$, which reduces M_{s1} .

Our getting such a high value of M_{s1} is important because, just like Kang et al. (2002), we have found in Section 3.1 that $M_{s1} \approx 10$ is a ‘breaking point’ in the thermal leakage model of particle injection: the injection rate depends weakly on M_{s1} when $M_{s1} \gtrsim 10$, but increases rapidly with decreasing M_{s1} if $M_{s1} < 10$.

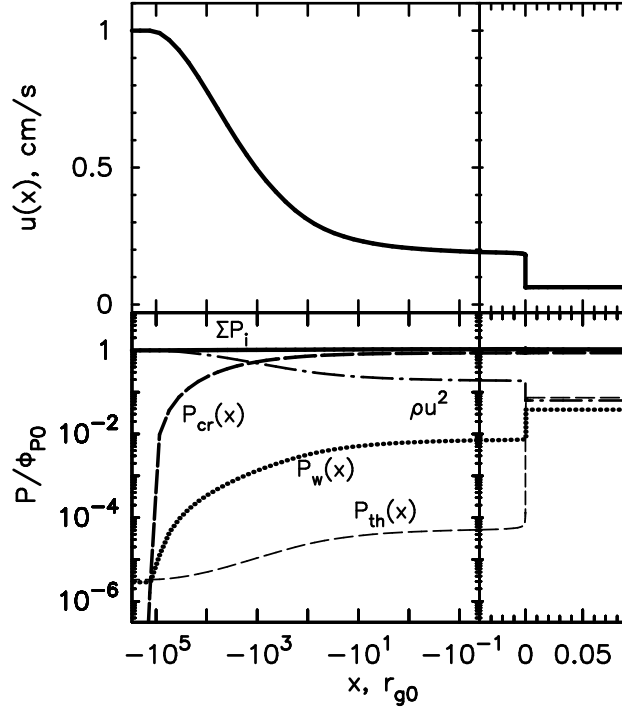


Fig. 6.— Illustration of momentum flux balance in the non-linear simulation with $\alpha_H = 0$ in the cold ISM case. The thin dashed line is the thermal pressure $P_{\text{th}}(x)$, the thick dashed line - the CR pressure $P_{\text{cr}}(x)$, the dotted line is the magnetic turbulence pressure $P_w(x)$, the dash-dotted line is the dynamic pressure $\rho(x)u^2(x)$, and the thick solid line is the sum of the four, the total momentum flux. All quantities are normalized to the far upstream value of the total momentum flux.

As an illustration for the above discussion, we show in Figure 6 the various constituents of the momentum flux across the shock with $\alpha_H = 0$ in the cold ISM ($T_0 = 10^4$ K) case. It's clear that upstream of the shock the dominant contributor to the momentum flux is the CR pressure $P_{\text{cr}}(x)$ and, therefore, the precursor compression is mainly determined by $P_{\text{cr}}(x)$. For this particular set of parameters, $P_{\text{cr}}(x)$ results in a decrease in the flow speed $u(x)$ by a factor of ~ 5.4 from its upstream value u_0 to the pre-subshock value u_1 . The temperature in the precursor only increases adiabatically for $\alpha_H = 0$ and this results in an increase over the far upstream temperature $T_1/T_0 \approx 3.3$, thus reducing the local sonic Mach number to $M_{\text{s1}} \approx 44$.

The subshock compression ratio r_{sub} is determined by the change in the different constituents of the momentum flux across the subshock. $P_{\text{cr}}(x)$, although large, changes little across the subshock¹², and what determines r_{sub} is the change in $P_{\text{th}}(x)$ and $P_w(x)$. The latter, as the plots in Figure 6 show, contributes significantly to the momentum flux. This is an important point because the values of B_{eff2} and $P_w(x)$ depend on r_{sub} and r_{tot} in a non-linear way making the traditional Rankine-Hugoniot relations inapplicable for determining r_{sub} . Relation (D10) can be used to iteratively calculate the resulting compression ratio r_{tot} , and it results in $r_{\text{tot}} = 16$ and $r_{\text{sub}} = 2.95$, as Table 1 shows. As we can see, the effect of magnetic turbulence pressure tends to decrease r_{sub} compared to the case $P_w(x) \ll P_{\text{th}}(x)$ (as in the latter case one would expect $r_{\text{sub}} \approx 4$ for $M_{\text{s1}} \approx 44$).

REFERENCES

- Achterberg, A., & Blandford, R. D. 1986, MNRAS, 218, 551
- Amato, E., & Blasi, P. 2006, MNRAS, 371, 1251
- Bamba, A., Yamazaki, R., Ueno, M., & Koyama, K. 2003, ApJ, 589, 827
- Baring, M. G., Ogilvie, K. W., Ellison, D. C., & Forsyth, R. J. 1997, ApJ, 476, 889
- Bell, A. R. 1978, MNRAS, 182, 147
- . 2004, MNRAS, 353, 550
- Bell, A. R., & Lucek, S. G. 2001, MNRAS, 321, 433

¹² $P_{\text{cr}}(x)$ is discontinuous at $x = 0$ in our simulation due to the contribution to it of the particles that have crossed the shock only a few times. The jump in $P_{\text{cr}}(x)$ in this case is small compared to the jump in thermal and magnetic pressures across the subshock, but can be significant for $\alpha_H > 0$, as seen in Figure 4.

- Berezhko, E. G., & Ellison, D. C. 1999, *ApJ*, 526, 385
- Berezhko, E. G., Ksenofontov, L. T., & Völk, H. J. 2003, *A&A*, 412, L11
- Blandford, R., & Eichler, D. 1987, *Physics Reports*, 154, 1
- Blasi, P., Gabici, S., & Vannoni, G. 2005, *MNRAS*, 361, 907
- Bykov, A. M. 1982, *Soviet Astronomy Letters*, 8, 320
- Bykov, A. M., & Topygin, I. N. 2005, *Astronomy Letters*, 31, 748
- Caprioli, D., Blasi, P., Amato, E., & Vietri, M. 2008, *ArXiv e-prints*, 804
- Cowsik, R., & Sarkar, S. 1980, *MNRAS*, 191, 855
- Ellison, D. C. 1982, *Ph.D. Thesis*
- . 1985, *J. Geophys. Res.*, 90, 29
- Ellison, D. C., Blasi, P., & Gabici, S. 2005, *proc. 29th ICRC (Puna, India)*
- Ellison, D. C., Giacalone, J., Burgess, D., & Schwartz, S. J. 1993, *J. Geophys. Res.*, 98, 21085
- Ellison, D. C., Jones, F. C., & Eichler, D. 1981, *Journal of Geophysics Zeitschrift Geophysik*, 50, 110
- Ellison, D. C., Jones, F. C., & Reynolds, S. P. 1990a, *ApJ*, 360, 702
- Ellison, D. C., & Moebius, E. 1987, *ApJ*, 318, 474
- Ellison, D. C., Moebius, E., & Paschmann, G. 1990b, *ApJ*, 352, 376
- Ellison, D. C., & Vladimirov, A. 2008, *ApJ*, 673, L47
- Giacalone, J. 2004, *ApJ*, 609, 452
- Giacalone, J., & Ellison, D. C. 2000, *J. Geophys. Res.*, 105, 12541
- Jones, F. C., & Ellison, D. C. 1991, *Space Science Reviews*, 58, 259
- Jones, F. C., Jokipii, J. R., & Baring, M. G. 1998, *ApJ*, 509, 238
- Kang, H., Jones, T. W., & Gieseler, U. D. J. 2002, *ApJ*, 579, 337
- Kulsrud, R. M. 2005, *Plasma physics for astrophysics* (Princeton University Press)

- Malkov, M. A. 1998, *Phys. Rev. E*, 58, 4911
- Malkov, M. A., & Drury, L. 2001, *Reports of Progress in Physics*, 64, 429
- McKenzie, J. F., & Voelk, H. J. 1982, *A&A*, 116, 191
- Niemiec, J., Pohl, M., & Stroman, T. 2008, *ArXiv e-prints*, 802
- Pelletier, G., Lemoine, M., & Marcowith, A. 2006, *A&A*, 453, 181
- Reynolds, S. P., & Ellison, D. C. 1992, *ApJ*, 399, L75
- Spitkovsky, A. 2008, *ApJ*, 673, L39
- Uchiyama, Y., & Aharonian, F. A. 2008, *ApJ*, 677, L105
- Vink, J., & Laming, J. M. 2003, *ApJ*, 584, 758
- Vladimirov, A., Ellison, D. C., & Bykov, A. 2006, *ApJ*, 652, 1246
- Warren, J. S., Hughes, J. P., Badenes, C., Ghavamian, P., McKee, C. F., Moffett, D., Plucinsky, P. P., Rakowski, C., Reynoso, E., & Slane, P. 2005, *ApJ*, 634, 376
- Wentzel, D. G. 1974, *ARA&A*, 12, 71
- Winske, D., & Omid, N. 1996, *J. Geophys. Res.*, 101, 17287
- Zirakashvili, V. N., Ptuskin, V. S., & Voelk, H. J. 2008, *ArXiv e-prints*, 801